Acta Biomaterialia 128 (2021) 314–331

Contents lists available at ScienceDirect

Acta Biomaterialia

journal homepage: www.elsevier.com/locate/actbio

Full length article

Peptide-coated polyurethane material reduces wound infection and inflammation

Ann-Charlotte Strömdahl[a,1], Lech Ignatowicz[a,1], Ganna Petruk[a,1], Marta Butrym[a], Sebastian Wasserstrom[b], Artur Schmidtchen[a,c], Manoj Puthia[a,*]

[a] Division of Dermatology and Venereology, Department of Clinical Sciences, Lund University, Lund, SE 22184, Sweden
[b] Lund University Bioimaging Centre, Lund University, Lund, SE 22184, Sweden
[c] Copenhagen Wound Healing Center, Bispebjerg Hospital, Department of Biomedical Sciences, University of Copenhagen, Copenhagen, DK 2400, Denmark

ARTICLE INFO

Article history:
Received 2 September 2020
Revised 21 April 2021
Accepted 22 April 2021
Available online 2 May 2021

Keywords:
Wound
Host defense peptide
Lipopolysaccharide
Inflammation
Infection

ABSTRACT

There is an urgent need for treatments that not only reduce bacterial infection that occurs during wounding but that also target the accompanying excessive inflammatory response. TCP-25, a thrombin-derived antibacterial peptide, scavenges toll-like receptor agonists such as endotoxins and lipoteichoic acid and prevents toll-like receptor-4 dimerization to reduce infection-related inflammation *in vivo*. Using a combination of biophysical, cellular, and microbiological assays followed by experimental studies in mouse and pig models, we show that TCP-25, when delivered from a polyurethane (PU) material, exerts anti-infective and anti-inflammatory effects *in vitro* and *in vivo*. Specifically, TCP-25 killed the common wound pathogens, *Pseudomonas aeruginosa* and *Staphylococcus aureus*, in both *in vitro* and *in vivo* assays. Furthermore, after its release from the PU material, the peptide retained its capacity to induce its helical conformation upon endotoxin interaction, yielding reduced activation of NF-κB in THP-1 reporter cells, and diminished accumulation of inflammatory cells and subsequent release of IL-6 and TNF-α in subcutaneous implant models *in vivo*. Moreover, in a porcine partial thickness wound infection model, TCP-25 treated infection with *S. aureus*, and reduced the concomitant inflammatory response. Taken together, these findings demonstrate a combined antibacterial and anti-inflammatory effect of TCP-25 delivered from PU *in vitro*, and in mouse and porcine *in vivo* models of localized infection-inflammation.

Statement of significance

Local wound infections may result in systemic complications and can be difficult to treat due to increasing antimicrobial resistance. Surgical site infections and biomaterial-related infections present a major challenge for hospitals. In recent years, various antimicrobial coatings have been developed for infection prevention and current concepts focus on various matrices with added anti-infective components, including various antibiotics and antiseptics. We have developed a dual action wound dressing concept where the host defense peptide TCP-25, when delivered from a PU material, targets both bacterial infection and the accompanying inflammation. TCP-25 PU showed efficacy in *in vitro* and experimental wound models in mouse and minipigs.

1. Introduction

The use of prophylactic systemic antibiotics can reduce the incidence of wound and surgical infections [1]. However, a rise in infections caused by antibiotic resistant strains of *Staphylococcus aureus* and *Pseudomonas aeruginosa,* bacterial species commonly found in wound and biomaterial-related infections, presents a major challenge [2,3]. In recent years, various antimicrobial coatings have been developed for infection prevention [4]. Current concepts focus on various matrices, such as synthetic or endogenous polymers, with added anti-infective components, including various antibiotics, or antiseptics, such as iodine, silver, polyhexamethylene biguanide, or chlorhexidine [5,6].

* Corresponding author.
E-mail address: manoj.puthia@med.lu.se (M. Puthia).
[1] These authors contributed equally to this work.

https://doi.org/10.1016/j.actbio.2021.04.045

Wound repair involves multiple biological processes, in which an initial hemostatic and inflammatory phase is followed by a regenerative phase and wound maturation. In most cases, the wound repair process leads to restoration of tissue integrity and function. It is well established that macrophages and neutrophils are critical for proper infection control and wound-healing responses. However, excessive recruitment of these leukocytes can negatively influence wound repair by increasing proteolysis and matrix degradation and causing cell senescence [7,8]. Inflammation is a complex process involving chemokines, growth factors, cytokines, proteases, antiproteases, and multiple cell types that all work in a controlled manner during the healing process. If this timely process is interrupted, a dysfunctional inflammatory phase occurs that is not seen in normally healing wounds. Toll-like receptors (TLR), so crucial for normal wound repair, can become over-activated in wounds and induce local dysfunctional inflammation which delays wound healing [9]. This may impair healing, increase susceptibility to infections, worsen scarring at a local level, and induce a systemic acute response [10,11]. There is compelling experimental evidence suggesting that control of dysfunctional inflammation might be therapeutically useful [12–15]. Current anti-infective treatments, either being incorporated in wound dressings for external application, or biomaterials and sutures for internal use, primarily target microbes and do not address the excessive inflammation that is associated with bacterial infection. However, this inflammation has the potential to cause various negative outcomes in patients such as delayed healing, erythema, pain, and fibrosis, despite complete microbial eradication. Hence, there is an unmet need for new treatment concepts that not only target the microbe, but also the accompanying early inflammatory process.

Thrombin-derived C-terminal peptides (TCP) are generated in response to wounding. Multiple TCPs exist in wounds, from larger-10 kDa forms which aggregate bacteria and endotoxins [16], to smaller forms of about 2 kDa [17,18], which exert dual anti-infective and anti-endotoxic effects [19,20]. A prototypic 25-amino acid TCP sequence (TCP-25, GKYGFYTHVFRLKKWIQKVIDQFGE), encompassing previously detected endogenously generated C-terminal peptides [21] showed therapeutic potential in experimental models of infection and endotoxic shock [19,20]. The peptide's mode of action involves direct binding to endotoxin and simultaneous interactions with monocytes and macrophages *in vitro* and *in vivo*, preventing CD-14 mediated signaling, toll-like receptor (TLR)-4 dimerization, and subsequent downstream endotoxin-induced pro-inflammatory cytokine responses [18,22]. Moreover, the peptide also inhibits TLR4- and TLR2-induced NF-κB activation in response to several other microbe-derived agonists, including lipoteichoic acid (LTA), peptidoglycan (PGN), and zymosan [22]. Previous studies investigated the effects of systemic administration of TCP-25 on invasive infection and related systemic inflammation [19,20]. In a recent study, using a neutral polymer (hydroxyethyl cellulose, HEC), we developed a hydrogel functionalized with TCP-25 [23]. We showed that the hydrogel enabled the dual function of TCP-25, targeting both bacteria and the accompanying inflammatory responses. Hydrogels provide hydration to the wound, can easily be used on larger surface areas, and may protect the drug from the hostile environment.

However, as many surgical and wound indications employ the use of biomaterials including dressings, it remained to be explored whether TCPs could be delivered from a biomaterial, thus conferring the material an ability to reduce *localized* infection-inflammation *in vivo*. If successful, this would provide a proof of concept whereby a given biomaterial or dressing can be functionalized enabling modulation at the tissue level of critical steps involved in the infection process. Here, in the context of surgery and wounding, utilizing mouse models of subcutaneous *S. aureus* and *P. aeruginosa* infections and a porcine partial thickness wound infection model, we therefore set out to explore whether localized delivery of TCP-25 *via* a hydrophilic polyurethane (PU) dressing material could constitute a new method for reducing both bacteria and inflammation, subcutaneously or when applied on wounds. Coated dressings are suitable for a prolonged drug release and are clinically useful where less frequent dressing changes are needed. Hydrogels are less suitable on exudative wounds, while PU dressing is an absorbent dressing which is clinically useful for acute or chronic exudative wounds. We here demonstrate a proof of concept that TCP-25 can indeed act as a dual-functional local anti-infective therapeutic when delivered from a PU material, targeting both bacteria and the accompanying inflammatory response.

2. Materials and methods

2.1. Peptides

The peptide TCP-25 (GKYGFYTHVFRLKKWIQKVIDQFGE) was synthesized by Ambiopharm (North Augusta, CS, USA). Tetramethylrhodamine (TAMRA)-, cyanine 3 (Cy3)-, cyanine 5 (Cy5)-, and cyanine 7 (Cy7)-labeled TCP-25 peptides were synthesized by Biopeptide Co. (San Diego, CA, USA). The purity (95%) of each peptide was confirmed by mass spectral analysis (MALDI-ToF Voyager).

2.2. Microorganisms

Bacterial strains used included *Escherichia coli* (ATCC 25922), *Pseudomonas aeruginosa* PAO1 and *Staphylococcus aureus* (ATCC 29213). For subcutaneous *in vivo* infection, bioluminescent *P. aeruginosa* Xen41 (PerkinElmer, Akron, OH, USA), and *S. aureus* SAP229 (kindly provided by Dr. Roger D. Plaut, Division of Bacterial, Parasitic, and Allergenic Products, FDA, Bethesda, Maryland, USA) were used. For wound infection in minipigs, *S. aureus* (ATCC 29213) was used.

2.3. Preparation of TCP-25 PU discs

A hydrophilic polyurethane (PU) foam dressing coated with a soft silicone layer was used for the study (Mepilex® Transfer, Mölnlycke Heath Care, Gothenburg, Sweden). Under sterile conditions, PU discs of 4 mm or 6 mm in diameter were generated using a biopsy punch (Kai). The peptide was solubilized in sterile water and stock solutions were made (5, 2.5, 2 and 1mg/mL). For coating, PU discs were kept in a petri dish and 20 µL from the stock solution was added to each PU disc. Control discs were coated with only 20 µL of sterile water. The petri dish was kept open in a class II biosafety cabinet while discs were air dried at room temperature (20°C ±1°C) for 12 h. Unless otherwise indicated, the final amount of peptide per 4 and 6 mm disc was 50 and 100 µg, respectively. To study the effects of coating time on antimicrobial properties, PU discs were coated with 20 or 100 µg TCP-25 for 2, 4, 8, 24, or 48 h at room temperature. To study the effect of coating temperature on antimicrobial properties, PU discs were coated with 20 or 100 µg TCP-25 at 20, 37 or 50°C for 2 h. After coating, discs were immediately stored at −80°C in a moisture free box.

For the wound study in minipigs, 4.5 × 4.5 cm pieces of PU dressing were cut under sterile conditions. Each PU piece was then transferred to a petri dish. TCP-25 was solubilized in sterile water and added to the PU dressing pieces (7.2 mg TCP-25 in 3 mL water for each piece). PU dressings were air dried overnight at room temperature (20°C ±1°C) in a class II biosafety cabinet. Three mL of sterile water was added to control PU dressings.

2.4. Radial diffusion assay (RDA)

Bacteria were grown to mid-logarithmic phase in 10 mL of full-strength (3% w/v) tryptic soy broth (TSB; Becton Dickinson) and

washed once in 10 mM Tris, pH 7.4. Bacteria (4×10^6 bacterial colony forming units [CFU]) were added to 15 mL of an underlay agarose gel consisting of 0.03% (w/v) TSB, 1% (w/v) low electroendosmosis type (EEO) agarose (Sigma-Aldrich, St Louis, MO) and 0.02% (v/v) Tween 20 (Sigma-Aldrich), and the mixture was poured into 144 mm petri dishes. Once the agarose underlay had solidified, 4 mm-diameter wells were punched and 6 µL of test sample was added to each well. 4 mm PU discs coated with 0, 2, 5, 10, 20, 50 and 100 µg TCP-25 were used in this assay. Three types of samples were used: freshly made TCP-25 PU discs, TCP-25 PU discs stored in dark for seven days at room temperature, and as control TCP-25 in buffer. To elute the peptide, TCP-25 PU discs were soaked in 200 µL of Tris buffer containing NaCl (10 mM Tris, pH 7.4, 0.15 M NaCl) and placed at 37°C in an incubator on shaking. After incubation for either 10 min or 2 h, 6 µL of each sample was used in the RDA assay. RDA plates were incubated at 37°C for 3 h to allow diffusion of the peptides. The underlay gel was then covered with 15 mL of molten overlay (6% TSB and 1% low-EEO agarose in distilled H_2O). Antibacterial activity of a peptide was visualized as a clear zone around each well after 18–24 h of incubation at 37°C. The activities of the peptides are presented as clear zone-to-well diameter (excluding the 4 mm well).

2.5. Peptide release assays

Two *in vitro* assays were used to measure the release of TCP-25 from the PU discs. In the first *in vitro* release assay, PU discs were coated with 50 µg TCP-25 (mixed with 2% TAMRA-labeled TCP-25). TCP-25 PU discs were eluted in a range of elution solutions. Cumulative release of TCP-25 was measured in the elution solution after taking out discs. In a 96-well black polystyrene plates (plate A), 4 mm PU discs coated with 50 µg TCP-25 (mixed with 2% TAMRA-labeled TCP-25) were placed in 200 µL of Tris buffer containing NaCl (10 mM Tris, pH 7.4, 0.15 M NaCl), deionized water, or 10% human plasma in Tris-NaCl buffer. Plates were covered, sealed with film to prevent evaporation and kept at 37°C with shaking (500 rpm). At the indicated time points, using tweezers, PU discs were taken out of the well and placed in a new empty 96-well black polystyrene plate (plate B). Immediately after, fluorescence intensity in the wells of both plates (plate A and plate B) was measured using the *In vivo* Imaging System (IVIS, PerkinElmer). Data was acquired using 560 nm excitation paired with a 600/20 nm narrowband filter. PU discs from plate B were then immediately returned to the elution solution in their respective wells in plate A. Again, plate A was kept at 37°C with shaking (500 rpm). This process was repeated for the indicated time points (i.e. 3, 6, 10, 20, 30, 60, 120, 180, 360 min). Each time, a new plate B was used to measure disc fluorescence. Plate A was used repeatedly and therefore showed cumulative TCP-25 TAMRA release in the elution solution. Values were expressed as a percentage of the relative fluorescence in the PU-disc and cumulative release in the elution solution after washing, compared to the fluorescence of the same peptide in standard solution (i.e. 50 µg peptide in 200 µL of medium was defined as 100%). The standard solution was treated in the same way as the elution buffer samples and fluorescence was measured with the same wavelengths.

In second *in vitro* release assay, a wound scenario was mimicked as described previously with some modifications [24,25]. In a 24-well plate, a transwell insert system (ThinCerts™, greiner bio-one, 3µm pore size) was used and a TCP-25 PU disc (coated with 100 µg TCP-25) was placed on top of the porous membrane in the upper compartment. The lower compartment was filled with 300 µL of elution solution (10 mM Tris, pH 7.4). Elution solution was in contact with porous membrane and the lower side of the TCP-25 PU (as illustrated in the cartoon in Fig. 1 B). The plate was covered with a lid and sealed to prevent evaporation. The whole setup was kept at 37°C on a shaker (60 rpm). From the lower compartment, a 20 µL sample was taken at each time point and immediately replenished with 20 µL of fresh elution solution. Samples were analyzed by measuring absorbance at 280 nm (A280) in a spectrophotometer (NanoDrop, Thermofisher) for the released TCP-25. Results were expressed as cumulative TCP-25 release (mg/mL). Complete elution of the peptide (0.33 mg/mL) was defined as the maximum concentration (C_{max}).

2.6. Circular dichroism (CD) spectroscopy

The change in secondary structure of free or LPS-bound TCP-25 was assessed by using a Jasco J-810 spectropolarimeter (Jasco, USA) equipped with a Jasco CDF-426S Peltier set to 25°C. The cell path length was 0.2 cm (Hellma, GmbH & Co, Germany). The spectrum was recorded in the far-UV range between 190–260 nm (20 nm/min scan speed). Each spectrum was the average of five scans with the background of the buffer solution subtracted. The concentration of the peptide was 10 µM, and the LPS concentration was 100 µg/mL. Before acquiring the spectrum, TCP-25 was incubated with LPS for 30 min at 37°C. Raw spectra were corrected for buffer contribution, with or without LPS, and converted to mean residue ellipticity, θ (mdeg cm^2 dmol^{-1}). The amount of α-helical structure was determined following the equation as reported previously [26].

2.7. Intrinsic fluorescence analysis

The binding of LPS to TCP-25 was measured by recording the intrinsic fluorescence of the peptide. 10 µM TCP-25 eluted from PU as reported above then diluted in sterile water at 10 µM and titrated with increasing lipid concentration (from 0.2 to 50 µg/mL). After excitation at 280 nm, the emission fluorescence spectra were recorded in the range 300–450 nm. Measurements were carried out at 25°C in a 3×3 mm cell by using a Jasco J-810 spectropolarimeter equipped with a FMO-427S fluorescence module. Emission spectra were acquired at a scanning speed of 150 nm/min, with 5 nm slit width and then smoothed by using 5 passes of binomial Gaussian. The LPS-binding affinity to the peptide was assessed by plotting the change in emission maxima (λ_{max}) as a function of different LPS concentrations. K_d was calculated by using GraphPad Prism v8.3.0 assuming a single binding site.

2.8. Viable-count assay (VCA)

Bacteria were grown to mid-logarithmic phase in Todd-Hewitt (TH) media, washed, and diluted with 10 mM Tris, pH 7.4 containing 0.15 M NaCl. Bacteria were then incubated at 37°C for 2 h with PU discs coated with or without TCP-25 (50 µg) in buffer only (10 mM Tris, 150 mM NaCl, pH 7.4) or with buffer supplemented with either 20% human plasma or 20% acute wound fluid. To quantify antimicrobial activity, various dilutions of reaction mixtures were plated on TH broth agar and incubated overnight at 37°C. Viability was quantified by counting CFU; the survival of treated bacteria is expressed in comparison to bacteria incubated with buffer, with or without supplements. To determine TCP-25 mediated killing of bioluminescent *P. aeruginosa* and *S. aureus, P. aeruginosa* Xen41 and *S. aureus* SAP229 bacteria were grown to mid-logarithmic phase in Todd-Hewitt (TH) media, washed and diluted with 10 mM Tris, pH 7.4 to obtain 2×10^7 CFU/mL. *P. aeruginosa* PAO1 and *S. aureus* ATCC 29213 were included for comparison. The bacteria were incubated at 37°C for 2 h with or without TCP-25 (100 µg) in 10 mM Tris, pH 7.4 and were then plated on THA (Todd-Hewitt Agar) plates and incubated overnight at 37°C.

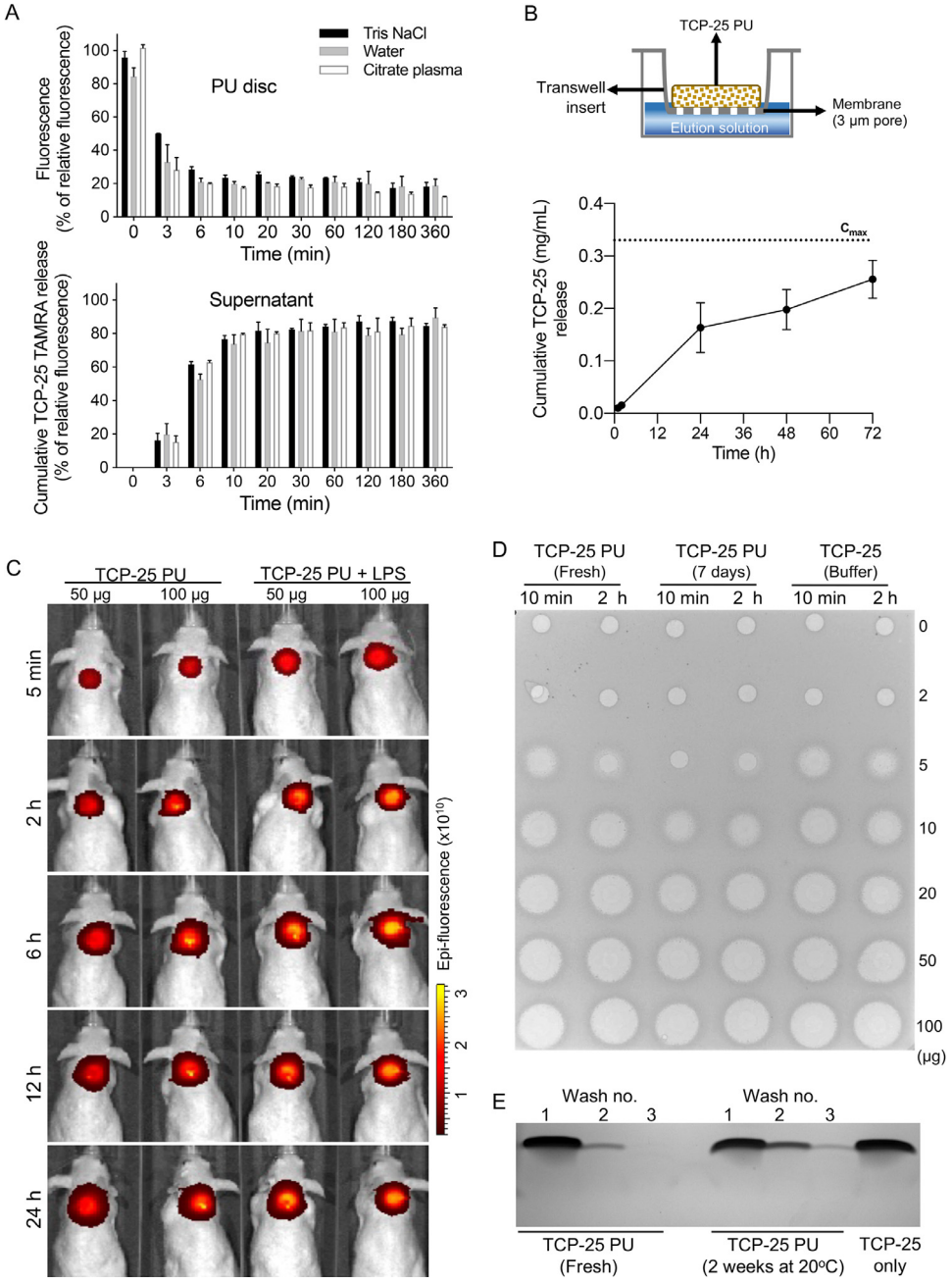

Fig. 1. Release, stability and antibacterial profile of TCP-25 peptide-coated PU dressing. (A) Peptide release profile from PU discs coated with fluorescently labeled TCP-25. PU discs were completely submerged in the buffer during the experimental setup. Release was measured by analysis of fluorescence intensity of the run off samples after serial washing. The relative amount of peptide remaining in the supernatant after washing compared to the corresponding peptide in solution only is indicated as % of relative fluorescence intensity. Data are represented as the mean ± SEM (n=3). (B) Cumulative release profile of TCP-25 peptide from PU discs *in vitro*. As shown in the cartoon, a transwell insert with 3 µm pore size membrane was used to obtain conditions mimicking a wound, with fluid only in contact with one side of the PU disc. C_{max}, concentration at which 100 % of TCP-25 is eluted. (C) Release of TCP-25 from PU discs *in vivo*. PU discs coated with Cy5-labeled TCP-25 were subcutaneously implanted in mice and release was evaluated by measuring fluorescence intensity using an IVIS bioimaging system. Representative light emission intensity heat-map overlays are shown (n=3). (D) Peptide activity and release from TCP-25-coated PU discs as determined by radial diffusion assay. The representative figure illustrates the zones of clearance (n=3). (E) SDS-PAGE analysis of released peptide from PU discs. TCP-25 dissolved in water was used as a positive control. A representative image is shown (n=3).

2.9. Antibacterial effects of TCP-25 PU on bioluminescent bacteria

Bioluminescent *P. aeruginosa* Xen41 and *S. aureus* SAP229 were grown to mid-logarithmic phase in TH media. The bacteria were washed for 20 min at 5600 rpm in 10 mM Tris (pH 7.4) and 1.3% glycerol buffer. The pellet was resuspended in 10 mM Tris buffer, and 200 µL from each strain (2×10^8 CFU/mL) was added to the 6 mm TCP-25 PU discs in a 96 well plate and incubated at 37°C. Bioluminescence was measured at 1, 5, 30, 60 and 120 min using an *in vivo* bioimaging system, IVIS® (Perkin Elmer).

2.10. NF-κB/AP-1 assay

NF-κB and AP-1 activation was assessed using THP1-Xblue™-CD14 reporter cells (here denoted as THP-1 cells) (InvivoGen, San Diego) according to the manufacturer's instructions. In brief, cells were grown in RPMI 1640 with 10% (v/v) heat-inactivated FBS, 1%

Antibiotic-Antimycotic (Invitrogen, Carlsbad, CA), 100 µg/mL G418 (InvivoGen, San Diego), and 200 µg/mL of Zeocin (InvivoGen, San Diego). After washing, 1×10^6 cells/well were placed into 24-well plates. 4 mm PU discs coated with 0, 2, 5, 10, 20, and 50 µg TCP-25 were used in this assay. TCP-25 PU discs were incubated in 500 µL buffer with *E. coli* LPS (O111:B4) (Sigma-Aldrich; approximate concentration 50 ng/mL) at 37°C for 1 h. After incubation, 20 µL from each sample was transferred into wells containing THP-1 cells and incubated at 37°C overnight. After overnight incubation, 20 µL of the media was transferred in a new 96-wells plate containing 180 µL QUANTI-Blue reagent (InvivoGen) and incubated at 37°C for 1-2 h. The level of secreted embryonic alkaline phosphatase (SEAP), an indicator of activation of transcription factors NF-κB and AP-1, was measured at OD 600 nm.

2.11. MTT assay

Sterile filtered MTT (3-(4,5-dimethyl-2-thiazolyl)-2,5-diphenyl-2H-tetrazolium bromide; Sigma-Aldrich) solution (5 mg/mL in PBS) was stored at -20°C protected from light until usage. Twenty µl/well of the MTT solution was added to the THP-1 cells from the abovementioned NF-κB/AP-1. Plates were incubated for 90 min in 5% CO_2 at 37°C. After incubation, the plates were centrifuged at 300 × g for 10 min and MTT-containing media was removed by aspiration. The blue formazan product was dissolved by the addition of 100 µL of 100% DMSO (Applichem, Germany) per well. The plates were then gently swirled for 30 min at room temperature to dissolve the precipitate and absorbance was read at 550 nm. Results represent mean values from triplicate measurements.

2.12. SDS-PAGE

4 mm PU discs coated with 100 µg TCP-25 were stored in dark at room temperature for 2 weeks. To elute the peptide, 200 µl of 10 mM Tris buffer with 1.3% glycerol was added to the tubes containing one disc and tubes were then agitated at 1400 rpm for 10 min at room temperature. Discs were placed inside 2 mL syringes and squeezed to extract buffer. Discs were then transferred to new tubes with 200 µL buffer, agitated at 1400 rpm for 10 min at room temperature, and again squeezed to extract buffer. This extraction process was repeated once more. From each washing, 4 µL of extracted buffer (equal to approximately 2 µg of TCP-25) was run on a 10–20% Tris-Tricine gel for 65 min at 125 V. As a control, 2 µg of TCP-25 was used. Gels were stained with Coomassie Brilliant Blue and visualized using a Gel Doc Imager (Bio-Rad Laboratories, Hercules, CA)

2.13. Scanning electron microscopy (SEM)

Bacteria were grown to mid-logarithmic phase in Todd-Hewitt (TH) medium, washed, and diluted with 10 mM Tris, pH 7.4 containing 0.15 M NaCl. Bacteria (100 µL, 2×10^7 CFU/mL) were then incubated at 37°C for 15 min with 4 mm PU discs coated with or without TCP-25 (50 µg). Samples were first washed twice in 0.1 M Sorensenś phosphate buffer pH 7.4 to remove media, then fixed in approximately 10 times the sample volume of "SEM fix" (0.1 M Sorensonś phosphate buffer pH 7.4, 2% formaldehyde and 2% glutaraldehyde) at room temperature for 15-20 min. After fixation, samples were washed twice in 0.1 M Sorensonś buffer pH 7.4 to remove excess fixative. Samples were then dehydrated in a graded series of ethanol (50, 70, 80, 90 and twice in 100%), critical point dried and mounted on 12.5 mm aluminum stubs and subsequently sputtered with 10 nm Au/Pd (80/20) in a Quorum Q150T ES turbo pumped sputter coater and examined in a Jeol JSM-7800F FEG-SEM.

2.14. Release of TCP-25 from PU discs in vivo

SKH-1 hairless mice (10–12 weeks old males) were anesthetized using a mixture of 2% isoflurane (Baxter) and oxygen. Under aseptic conditions, an approximately 10 mm cut was made on the skin of mouse's back and the tip of the scissors was used to create a small pocket. To image *in vivo* peptide release, discs coated with Cy5-labeled TCP-25 were inserted in the subcutaneous pocket and the wound was closed with suture (VICRYL™, Johnson & Johnson, Belgium). The release of peptide was evaluated by measuring fluorescence intensity using an *in vivo* imaging system (IVIS). To study the effect of LPS contamination on TCP-25 release, wounds were contaminated by adding 1 mg LPS/kg body weight in 50 µL of PBS buffer to each PU disc.

2.15. Pharmacokinetics in mouse model of deep partial-thickness burn wounds

Female BALB/c mice, 10-11 weeks old, were used to study pharmacokinetics of TCP-25 PU in a deep partial-thickness burn wound model. Burn wounds were induced as described previously with minor modifications [27]. 30 min before the induction of the injury, for pain relief, the mouse was given buprenorphine (0.1 mg/kg) subcutaneously. The mouse was anaesthetized with combination of ketamine (80 mg/kg) and xylazine (10 mg/kg) intraperitoneally. The hair on the back of the mouse were removed using depilatory cream and then cleaned with a damp gauze. The mouse was placed in a polypropylene template that exposed the shaved back and 6% of the body surface. The template was then placed in 54°C water for 20 s in such a way that only the exposed area on the back came into contact with the water. The mouse was removed from the template and the burn area was dabbed with moistened paper towels and dried with gauze. For resuscitation, the mouse was given 1 mL of pre-warmed Ringer's lactate solution subcutaneously. The mouse was allowed to recover on a heating pad. PU discs coated with 50 µg of TCP-25 were placed on the burn wound and covered with a secondary dressing (Tegaderm, 3M™). TCP-25 PU discs were removed from the wound 2, 6, 24, 48 and 72 h after their application and eluted in Tris buffer (10 mM Tris, pH 7.4). Elution samples were frozen at −80°C and used for further analysis by HPLC, Western blot and RDA.

For longitudinal *in vivo* fluorescence imaging, PU discs coated with 50 µg of TCP-25 (mixed with 2% Cy3-labeled TCP-25) were placed on the burn wound and covered with Tegaderm secondary dressing. The pharmacokinetics of peptide was evaluated by measuring fluorescence intensity using the IVIS spectrum. Whole body IVIS imaging was performed under isoflurane anesthesia 6, 24 and 48 h after the application of TCP-25 PU. The mice were imaged with the dressing and after removal of the dressing. In addition, the removed dressing was also imaged. After each time point, the mice were sacrificed and wound biopsies were snap frozen and mounted in optimal cutting temperature (OCT) compound (Sakura Finetek) for cryosectioning. Cryosections were washed once in PBS for 5 min at room temperature (RT) and counterstained with 4′,6-diamidino-2-phenylindole (DAPI) solution (0.5 mM in PBS; 1 min, RT). Slides were washed once in PBS for 5 min at RT and mounted with antifade mounting medium (PermaFluor, ThermoFisher Scientific). Sections were imaged using fluorescence microscopy (AxioScope.A1, Carl Zeiss).

2.16. Mouse model of subcutaneous infection

Bioluminescent strains of *S. aureus* and *P. aeruginosa* were used for the *in vivo* subcutaneous infection experiments. To prepare the bacterial inoculum, bacteria were grown to mid-logarithmic phase

in 10 mL of TB medium, washed, and resuspended to obtain suspensions of 10^5 CFUs in 50 µL. BALB/c mice (8–10 weeks old males) were anesthetized using a mixture of 2% isoflurane (Baxter) and oxygen. Under aseptic conditions, an approximately 10 mm cut was made on the skin of mouse's back and the tip of the scissors was used to create a small pocket. PU disc (6 mm) with or without TCP-25 was inserted in the pocket and 50 µL of bacterial suspension was then added to each PU disc. Skin wound was then closed with suture (VICRYL™, Johnson & Johnson, Belgium). At various time points, *in vivo* status of bacterial infection was longitudinally evaluated by measuring bioluminescence using the IVIS bioimaging system. At termination, tissue surrounding the PU material and PU discs were collected for further analyses. For CFU analysis, collected tissue and PU discs were homogenized and serial dilutions were plated on TH broth agar and incubated overnight at 37°C.

2.17. Mouse model of subcutaneous inflammation

BALB/c tg(NF-κB-RE-Luc)-Xen reporter mice (Taconic Biosciences, Albany, NY, USA), 10–12 weeks old males, were used to evaluate the anti-inflammatory effects of TCP-25 PU. Under aseptic conditions, an approximately 10 mm cut was made on mouse's dorsum and the tip of the scissors was used to create a small pocket. PU disc (6 mm) with or without TCP-25 was inserted in the pocket. Wounds were then contaminated by adding 1 mg LPS/kg body weight in 50 µL of PBS buffer to each disc implant and the wound was closed with suture. IVIS bioimaging was used for the longitudinal determination of NF-κB activation as a measure of inflammation. 15 min prior to IVIS imaging, mice were intraperitoneally injected with 100 µL of D-luciferin (PerkinElmer, 150 mg/kg body weight). Bioluminescent signals from the mice were acquired and quantified using Living Image 4.0 Software (PerkinElmer).

2.18. Preparation of cell suspension from skin tissue and implanted PU material

24 h post disc implantation, mice were sacrificed, fur was removed using a trimmer and 1 cm^2 skin samples were collected. Subcutaneous fat and muscles were removed from the skin by scraping. Separation of the epidermis and dermis was accomplished by floating the skin tissue overnight in DMEM media containing 0.2% dispase at 4°C. Dermal sheets were peeled off of the epidermis and washed in PBS for 10 min. Tissue was minced into small pieces using surgical scissors and digested in 1 mL DMEM media containing 0.25% collagenase type I (Worthington, Lakewood, NJ, USA) for 45 min at 37°C. Samples were vortexed every 15 min. The dermal cell suspension was filtered through a 70 µm cell strainer and washed twice in 500 µL of cold PBS (with centrifugation at 500 × g for 5 min between wash steps) before immunolabeling. Cell viability of dermal cell suspension was routinely found to be 70 to 80%, as determined by trypan blue exclusion.

To recover cells from PU, discs were removed from the subcutaneous space of the mice. Discs were collected in 1 mL PBS and kept on a shaker (200 rpm, 1 h, RT). Discs were discarded and infiltrating cells were collected by centrifugation of the supernatant (500 × g, 5 min). The cell pellet was resuspended in 500 µL of PBS and cells were counted in a Bürker chamber.

2.19. Flow cytometry

Cells recovered from skin were suspended in 50 µL of staining buffer (PBS buffer with 0.02% sodium azide and 5% heat-inactivated fetal calf serum) containing fluorochrome-conjugated antibodies (purchased from BD, Franklin Lakes, NJ, USA; eBioscience, Grand Island, NY, USA; or BioLegend, San Diego, CA, USA). The CD11b-AlexaFluor 647 (BioLegend) and Gr-1-AlexaFluor 488 (BioLegend) antibodies were used. Cells were incubated in the dark at room temperature for 30 min and washed once in staining buffer with centrifugation at 500 × g for 5 min. Thereafter, cells were incubated in staining buffer containing 0.25 µg 7-aminoactinomycin D (7-ADD) for 15 min in the dark and fixed with 0.5 % paraformaldehyde. Cells were separated using a FACSVerse flow cytometer (BD Biosciences, San Jose, CA, USA) and data were analyzed using FlowJo software (Tree Star, Inc., Ashland, OR, USA). The relative proportion of neutrophils or macrophages was expressed as a percentage of total viable cells. For the identification of various cell populations (gating scheme described in supplementary Fig. 9), forward versus side scatter (FSC Vs SSC) gating was used to identify cells and exclude debris. This was followed by excluding doublets (FSC-H Vs FSC-A). Next, 7-AAD negative cells were gated as live cells which were then followed by gating CD11b+ cells. Finally, GR-1 high (neutrophils) and GR-1 low (macrophages, monocytes) populations were gated.

2.20. Western Blot

TCP-25 PU discs (6 mm, coated with 100 µg TCP-25) removed from burn wounds in mice were placed in 50 µL of 10 mM Tris at pH 7.4 and stored at −20°C until analysis. Five µL from each sample was loaded on a 10–20% Tris-Tricine gel and run for 65 min at 125 V. PU disc coated with 100 µg TCP-25 and placed in 50 µL of 10 mM Tris at pH 7.4 was used as a control. At the end of the run, the material was transferred to a PVDF membrane using a Trans-Blot Turbo system (Bio-Rad, Laboratories, Hercules, CA, USA). TCP-25 was detected using polyclonal rabbit antibodies against the C-terminal thrombin epitope VFR17 (VFRLKKWIQKVIDQFGE; diluted 1:1000, Innovagen AB, Lund, Sweden), followed by porcine anti-rabbit HRP-conjugated antibodies (1:1000, Dako, Glostrup, Denmark). The peptide was visualized by incubating the membrane with SuperSignal West Pico Chemiluminescent Substrate (Thermo Scientific, Rockford, IL, USA) for 5 min, followed by detection using a ChemiDoc XRS Imager (Bio-Rad Laboratories, Hercules, CA, USA).

2.21. High-Pressure liquid chromatography (HPLC)

TCP-25 eluted from PU discs which had been removed from burn wounds in mice were analyzed by reverse-phase chromatography as reported previously [28]. Briefly, a Phenomenex Kinetex C18-column (50 × 2.1 mm 2.6 µM, 100 Å pore size, Torrance, CA, USA) was equilibrated using 95% of buffer A containing 0.25% of Trifluoroacetic acid (TFA) in MilliQ and 5% of buffer B containing 0.25% of TFA in acetonitrile. The peptide was dissolved in buffer A (1:4) and 10 µL was injected into the system. The elution profile was monitored during the gradient (35% of B at 5 min, 45% at 10 min), and the spectrum at 215 nm was recorded. The flow rate through the column was 0.5 mL/min, and all runs were performed at room temperature.

2.22. Hemolytic activity

PU discs (6 mm, coated with 100 µg TCP-25) were placed in tubes containing 225, 450 or 900 µL of RPMI-1640- GlutaMAX-I without phenol red (Gibco). After 10 min, fresh venous blood from healthy donors (collected in 50 µg/mL lepirudin tubes) was added at a final concentration of 25%. Hemolytic activity of uncoated PU was analyzed by putting a 6 mm PU disc in 225 µL of RPMI. Blood (25%) in RPMI with no disc was used as negative control, while 75 µL of blood mixed with 225 µL of 5% Tween-20 was a positive control. After incubation at 37°C with 5% CO_2 for 1 h, the tubes were

centrifuged at 800 × g. One-hundred-and-fifty µL of each sample was transferred to a flat-bottom transparent 96-well plate and the absorbance at 450 nm was measured. The percentage of hemolysis was calculated using the following formula:

$$\frac{\text{Abs 450 nm (Sample} - \text{control)}}{\text{Abs 450 nm (Posivite control} - \text{control)}} \times 100$$

2.23. Biological materials

Sterile wound fluids were obtained from surgical drainages after surgery. The collection of samples was performed 24–48 h after surgery. The wound fluids were centrifuged, aliquoted, and stored at −20°C.

2.24. Minipig partial thickness wound model

A minipig partial thickness wound model was used to study *S. aureus* wound infection *in vivo*. Surgical and infection procedures were performed by qualified veterinarians under strict aseptic conditions. Female Göttingen minipigs (14–16 kg body weight) were acclimatized for 1 week and off-fed the night before wounding. Using a hair trimmer, hair on their back was clipped 24 h before surgery. Procedures on the day of wounding and infection were performed under general anesthesia. For general anesthesia, minipigs were given Tiletamine and Zolacepam (Zoletil 50, Virbac, Sweden). Induction dose of anesthetic (Zoletil 1 mL/10 kg body weight) was given intramuscularly and maintained intravenously (Zoletil 0.5 mL/10 kg body weight). For respiratory support, minipigs were supplemented with oxygen *via* a facemask. Just before the surgery for wounding, the minipig's back was thoroughly cleaned with chlorhexidine (MEDI-SCRUB sponge; Rovers, Oss, Netherlands) and lukewarm water. Using a razor, the dorsum was shaved and disinfected with chlorhexidine solution (4%). Sterile gauze was then used to dry the area completely. A sterile scale ruler and tissue pen was used to mark wound outlines. An electric dermatome (Zimmer) was used to make 12 partial thickness (750 µm deep) wounds (2.5 × 2.5 cm) on the back (six wounds on each side). For the ease of dressing and to avoid cross contamination, a minimum distance of 4 cm was maintained between the wounds. Immediately after wounding with dermatome, wounds were covered with sterile gauze to prevent bleeding. To prepare bacterial inoculum for wound infection, overnight *S. aureus* (ATCC 29213) cultures were refreshed and grown to mid-logarithmic phase in TH medium. After washing bacteria for 15 min (5.6 × 1000 rpm), they were diluted with 10 mM Tris buffer (pH 7.4) to achieve a concentration of 2×10^8 CFU/mL. Inoculum was prepared by suspending bacteria in a 2% neutral polymer hydroxyethyl cellulose (HEC) hydrogel (10^7 CFU/100 µL hydrogel) and applied directly onto the fresh wound. After an interval of 15 min, TCP-25 PU or only PU dressing was applied to the wounds. The dressing was then covered with a transparent breathable fixation dressing (Mepore® Film; Mölnlycke, Gothenburg, Sweden) and secured using skin staples (SMI, St. Vith, Belgium). To provide better protection, the wound area was then covered with two layers of sterile cotton gauze and secured with adhesive tape. A final layer of flexible self-adhesive bandage (Vet Flex, Kruuse, Denmark) was applied over the dressings and around the body to secure the dressings underneath. Minipigs were housed individually and monitored daily. Dressing were changed every day under general anesthesia and observations were made. Wounds were documented by imaging and clinical scoring [23] was performed by a qualified veterinarian. For CFU analysis, swab samples were taken from the wound surface. Primary PU dressings were collected every day and wound fluid was recovered and further analyzed for cytokines. Minipigs were sacrificed 4 days after wounding and infection. Wound tissue samples were collected from minipigs on the day of termination.

2.25. Cytokine assay

To measure cytokine levels from the mouse model of subcutaneous inflammation, mice were euthanized at 8 and 24 h after PU disc implantation. PU discs were surgically recovered from the subcutaneous space. Discs were centrifuged in a modified spin column (1000 rpm) to retrieve fluid. The levels of IL-6, IL-10, IL-12, MCP-1, IFN-γ, and TNF-α were assessed in murine plasma or PU disc fluid using the Mouse Inflammation Kit (Becton Dickinson AB, Franklin Lakes, NJ, USA) according to the manufacturer's instructions. IL-1 and TGF-β were assessed using ELISA DuoSet® kits (R&D Systems, Minneapolis, MN, USA) according to the manufacturer's instructions. For minipig wound fluid analysis, PU dressings from the porcine wounds were transferred to a 5 mL pre-chilled tube and kept on ice. To extract wound fluid, dressings were soaked in 500 µL of cold 10 mM Tris buffer at pH 7.4 and centrifuged for 5 min (2000 × g, 4°C). Extracted wound fluids were aliquoted into pre-chilled Eppendorf tubes and stored at −80°C. To determine TNF-α concentrations in wound fluid, porcine TNF-α DuoSet® ELISA Kit (R&D Systems, Minneapolis, MN, USA) was used according to manufacturer's recommendations. If cytokine concentrations were higher than the maximum quantifiable level of the assay, samples were diluted (10 , 20 and 100 ×) and measured again.

2.26. Histology

Harvested skin derived from the implantation site on the mouse was placed on absorbent paper to prevent curling, then trimmed to 6-7 mm thick sections, which were fixed overnight in 4% paraformaldehyde and stored in 70% ethanol. For minipig wounds, tissue samples were fixed overnight in neutral buffered formalin and then stored in 70% ethanol. After serial dehydration, the tissue was embedded in paraffin blocks, sectioned at 5 µm, and stained with hematoxylin and eosin (H&E). Samples were imaged with bright field microscopy (Axioplan2, Zeiss, Germany) under 100 × and 200 × magnifications. For mouse tissue, four random microscopic views (100 ×) from each H&E-stained skin tissue section were scored for the extent of cellularity. Scoring was based on a scale of 0–5, with 0 being the lowest and 5 being the highest tissue cellularity. For minipig tissue, H&E-stained sections were examined and scored on a scale of 0-5 (where 0 is worse and 5 is best score) [23]. The histological scoring was based on epithelization, granulation tissue, inflammatory cells, abscesses and tissue architecture. For each wound tissue section, five areas were examined under 100 × magnification which covered 90–100% wound.

2.27. Immunohistochemistry

Skin tissue sections were deparaffinized, blocked in 1% BSA (Sigma-Aldrich), and stained with primary antibodies against neutrophils (NIMP-R14, ab2557, Abcam, Cambridge, MA, USA) and macrophages, respectively (RM0029-11H3, sc-101447, Santa Cruz, Dallas, TX, USA). Alexa 568 anti-rat IgG (Life Technologies, Carlsbad, CA) was used as the secondary antibody. Nuclei were counterstained with 4′,6-diamidino-2-phenylindole (DAPI; 0.05 mM, Sigma-Aldrich). Sections were imaged by fluorescence microscopy (AX60, Olympus Optical). Four random microscopic views (100 ×) from each immunostained skin tissue section were scored for the extent of neutrophilic infiltration. Scoring was based on a scale of 0–10, where 0 represented no neutrophil invasion and 10 represented the highest neutrophil infiltration. For macrophage count, four random microscopic views (100 ×) from each immunostained skin tissue section were used.

2.28. Ethics statement and gender considerations

All animal experiments were performed according to Swedish Animal Welfare Act SFS 1988:534 and were approved by the Animal Ethics Committee of Malmö/Lund, Sweden (permit numbers M252-11, M131-16, M88-91/14, M5934-19, 8871-19, M5935-19, 8643-20). The use of human wound materials was approved by the Ethics Committee at Lund University (LU 708-01 and LU 509-01). Informed consent was obtained from all of the donors, and the use of human blood was approved by the Ethics Committee at Lund University (permit no. 657–2008).

In the current animal experiments, robust models of infection and inflammation were used, and we expected potential gender differences in responses to microbial infection and endotoxins to be subtle. We used both male and female mice for different experiments. We have used female minipigs for our porcine wound model and do not expect significantly different responses in males.

2.29. Data analyses

Differences in the mean between two groups were statistically determined using Student's *t* test for normally distributed data and Mann-Whitney test otherwise. Means of more than two groups were compared using a one-way ANOVA with post hoc (Tukey) for normally distributed data or Kruskal-Wallis test with post hoc (Dunn's) were used otherwise. Data are presented as means ± SEM or SD. Clinical scoring of minipig wounds is shown as medians. Details of statistical analysis are indicated in each figure legend and GraphPad Prism software v8 was used. *P* values <0.05 were considered to be statistically significant.

3. Results

3.1. Functionalization of PU material with TCP-25, in vitro peptide release and structure

In a previous study, a human acellular dermal substitute was found to bind TCP-25, conferring the material anti-bacterial and anti-endotoxic effects, as well as reducing material-induced contact activation [29]. However, this work was *in vitro* based, and TCP-25 was significantly, and also to various extent, bound to the biological material. In an effort to design a topical dressing capable of fast, reproducible, and localized TCP delivery for subsequent *in vivo* studies, polyurethane (PU) discs were coated with TCP-25 peptide. PU was selected because of its hydrophilic characteristics, current use in foam dressings, and importantly, inert character [30]. In order to study the release of TCP-25, coated PU discs (spiked with TAMRA-labeled TCP-25) were eluted with either deionized water, isotonic Tris-buffer alone, or Tris-buffer with human citrate plasma. The results showed that the peptide was instantaneously released from the PU disc, yielding over 90% release after 10 min (Fig. 1A). Release of the peptide did not significantly differ between washing solutions (Fig. 1A). In this release assay, TCP-25 PU dressing was completely submerged in the elution buffer and did not represent the *in vivo* scenario where the dressing is applied topically on the wound and peptide exchange occurs only from the contact surface of the dressing. Therefore, next, we used an *in vitro* model that better mimics a skin wound scenario [24,25]. A transwell insert system was used and TCP-25 PU was kept on the porous membrane in the upper compartment. The lower compartment was filled with elution buffer. Elution buffer remained in contact with the porous membrane and the lower part of the TCP-25 PU (as illustrated in Fig. 1 B). The TCP-25 was released continuously for 72 h (Fig. 1 B). To determine release *in vivo*, PU discs were coated with Cy5-labeled TCP-25 peptide and subcutaneously implanted into hairless SKH-1 mice. The results showed that the peptide was released into the immediate implant surroundings and persisted for up to 24 h at the site, as assessed by bioimaging (Fig. 1C and Supplementary Fig. 1). Because TCP-25 shows a strong affinity to bacterial endotoxin and can act as a scavenger by binding to LPS [22] the effect of LPS on TCP-25 at the implanted PU material site was evaluated. The presence of LPS did not affect either the release of the peptide from the disc or its local retention (Fig. 1C and Supplementary Fig. 1).

A radial diffusion assay was employed to determine the activity and stability of the peptide released from the PU disc (Fig. 1D). Bacterial inhibition zones of discs incubated for 10 min and 2 h were similar in size, results indeed compatible with the rapid release of the peptide observed in Fig. 1A. Furthermore, the activity of the released peptide was similar to that of the peptide assayed in buffer alone, suggesting quantitative release of the peptide (Supplementary Fig. 2). In addition, sodium dodecyl sulfate polyacrylamide gel electrophoresis (SDS PAGE) analysis confirmed the release of TCP-25 from the PU material and demonstrated that released TCP-25 was not degraded (Fig. 1E and Supplementary Fig. 3). Moreover, influence of coating time and temperature on the antibacterial capacity of TCP-25 PU was investigated. Coating times of 2, 4, 8, 24, and 48 h showed significant antibacterial activity (Supplementary Fig. 4A). There were no significant differences in antibacterial activity between the different coating times. PU discs prepared at coating temperatures of 20, 37 and 50°C showed significant antibacterial activity and no significant change in activity was observed with change in coating temperatures (Supplementary Fig. 4B). PU discs coated with the higher amount (100 µg /PU disc) of TCP-25 showed relatively higher antibacterial activity than the discs coated with 20 µg of TCP-25 (Supplementary Fig. 4).

In order to determine if TCP-25 delivered from PU was still able to bind to LPS, the structural changes of the peptide were analyzed. Circular dichroism (CD) analysis showed that TCP-25 eluted from PU acquired a helical structure in the presence of LPS (Fig. 2A). This LPS-induced structural change determines the change in intrinsic fluorescence of the peptide when excited at 280 nm. Indeed, a shift in emission maximum (λ_{max}) to the left was observed, indicating the binding of LPS to the peptide (Fig. 2B). K_d (11.15±1.76 µg/mL) determined by fitting the λ_{max} of TCP-25 in function of different concentrations of LPS (Fig. 2C) was in agreement with previous results [18].

3.2. In vivo pharmacokinetics of TCP-25 PU in a mouse model of burn wounds

To investigate the *in vivo* pharmacokinetics of TCP-25 in a real wound situation, we used a mouse model of partial-thickness burn wounds which heals through slow contraction and re-epithelization and exhibits similarities to human partial-thickness burn wounds [31]. A deep partial-thickness burn wound was made on the dorsum of each BALB/c mouse. The wound was then dressed with TCP-25 PU. Thereafter, longitudinal IVIS imaging, HPLC, western blot, and tissue sectioning was employed to methodically investigate the pharmacokinetics of TCP-25 *in vivo*. The results from fluorescence IVIS imaging show that TCP-25 was released to and retained at the wound surface for at least 48 h (Fig. 3A).

Released TCP-25 was detected on the surface of the wound and in the wounded tissue at 6, 24 and 48 h (Fig. 3B). Furthermore, TCP-25 PU dressings were recovered from the wound and eluted for further analysis. The results show that a significant amount of intact TCP-25 was present in the PU discs even 48 h after application to the wound (Fig. 3C, D). Importantly, when eluted from the PU dressings recovered 6, 24, 48, and 72 h after application to the wounds, TCP-25 showed significant bioactivity (Fig. 3E). Taken together, these findings demonstrate that TCP-25 PU discs continu-

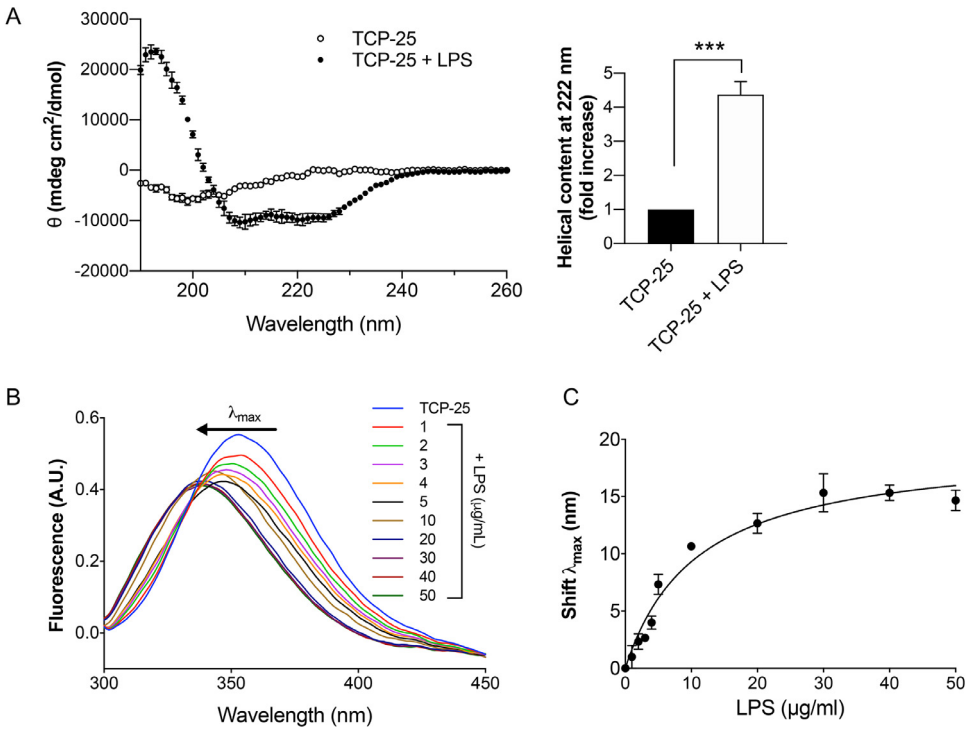

Fig. 2. Structural changes of TCP-25 determined by CD spectroscopy. (A) CD spectra of 10 μM TCP-25 eluted from PU disc alone or after incubation with 100 μg/mL LPS (left panel). α-helical content of TCP-25 calculated from molar ellipsometry at 222 nm (right panel). Data are represented as the mean ± SEM (n=3). P value was determined using an unpaired t test. (B) Representative spectra of intrinsic fluorescence of 10 μM TCP-25 eluted from PU discs, indicating shifts in the emission maximum of the peptides upon incubation with increasing concentration of LPS in deionized water (left panel). (C) Fitting of the emission maximum wavelength (λ_{max}) of TCP-25 in function of different concentrations of LPS. Data are represented as the mean ± SEM (n=3). $^{***}P < 0.001$.

ously release a significant amount of TCP-25 to the wound site for at least 48 h. Moreover, results show that TCP-25 is retained in PU discs for at least 72 h and remains bioactive.

3.3. *TCP-25-functionalized PU-discs exert antibacterial properties* in vitro

The antimicrobial efficacy of TCP-25 PU was then evaluated *in vitro* using a viable count assay with reference strains of *S. aureus* and *P. aeruginosa* and a laboratory strain of *E. coli* that had been incubated with PU discs with or without TCP-25. The assay was performed in buffer alone or buffer supplemented with 20% human plasma or 20% acute wound fluid. Importantly, the TCP-25 PU discs displayed significant antimicrobial activity in both plasma and wound fluid when compared with the control discs without peptide (Fig. 4A). Next, bioluminescent *P. aeruginosa* and *S. aureus* were used to demonstrate antibacterial efficacy. As illustrated using luminescence imaging (Fig. 4B), the peptide-functionalized PU yielded a rapid reduction in *P. aeruginosa* and *S. aureus* bioluminescence already after 1 min of incubation. Scanning electron microscopy was employed to further study effects of TCP-25 PU on *P. aeruginosa* or *S. aureus*. In contrast to the untreated PU discs, bacteria on PU functionalized with TCP-25 showed clear morphological changes and a significant amount of bacterial intracellular material was present extracellularly, indicating bacterial lysis (Fig. 4C and Supplementary Fig. 5). In TCP-25 PU discs, bacterial clumping and debris were observed, which were absent in control PU discs. Bacteria in control PU discs showed smooth cell wall surfaces whereas small perturbations were observed on bacterial surfaces in the TCP-25 PU group. These morphological changes were consistent with our previous observations [20,32]. Taken together, these results demonstrate that TCP-25 retains its antibacterial activity in the PU material, exerting a rapid killing effect.

3.4. *TCP-25-functionalized PU-discs are antibacterial in an experimental mouse model of subcutaneous infection*

Next, we employed a mouse model mimicking a situation of surgical contamination [23] with bioluminescent strains of *P. aeruginosa* and *S. aureus*. Similar to the isolates used above, these bacteria were killed by TCP-25 *in vitro* (Supplementary Fig. 6). PU discs alone or those coated with TCP-25 were subcutaneously implanted into BALB/c mice. Discs were contaminated at the site of implantation with 10^5 CFU of bioluminescent *P. aeruginosa* and *S. aureus*. To study the effects of TCP-25 at the early phase of infection, longitudinal *in vivo* imaging was performed using IVIS bioimaging. Bioluminescence intensity decreased significantly in all mice that received TCP-25 compared with control mice (Fig. 5A, B). After an incubation period of 24 h, significantly reduced levels of viable *P. aeruginosa* and *S. aureus* bacteria were observed in the surrounding tissue as well as the implanted PU discs (Fig. 5C) after treatment with TCP-25.

3.5. *TCP-25 functionalized PU material blocks endotoxin-induced inflammation* in vitro *and* in vivo

The ability for TCP-25-coated discs to suppress LPS-triggered inflammation was then explored using both *in vitro* and *in vivo* models. THP1-XBlue™-CD14 cells [22,33] were stimulated with *E. coli* LPS in the presence of TCP-25-coated PU discs, resulting in a significant dose-dependent inhibition of LPS-induced TLR-driven inflammatory cascade (Fig. 6A). Importantly, the concentration of TCP-25 that yielded these results did not cause cell toxicity as assessed by MTT assay.

For evaluation of local anti-endotoxic effects of TCP-25 PU *in vivo*, PU discs alone or those coated with TCP-25 were contami-

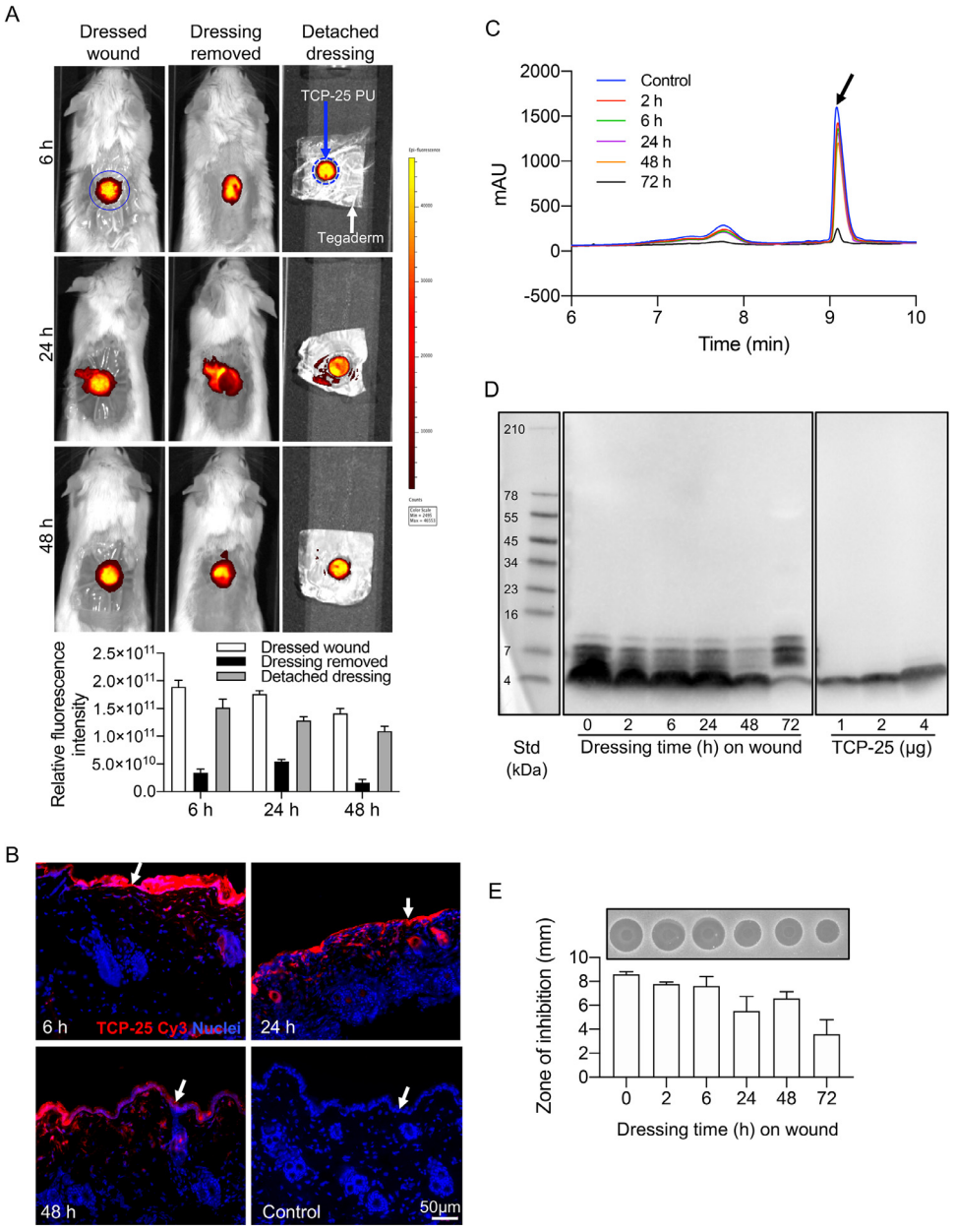

Fig. 3. *In vivo* pharmacokinetics of TCP-25 PU in a mouse model of burn wounds. A mouse model of deep partial-thickness burn wounds was employed to study *in vivo* release and pharmacokinetics. A burn wound was made on the dorsum of BALB/c mice, dressed with TCP-25 PU or TCP-25 (labeled with Cy3) PU, and covered with a transparent film dressing. (A) For study of pharmacokinetics *in vivo*, wound dressed with TCP-25 (labeled with Cy3) PU were analyzed by longitudinal *in vivo* fluorescence imaging using the IVIS spectrum. The mice were imaged with the dressing and after removal of the dressing. The removed dressing was also imaged. Representative images show distribution of TCP-25-Cy3 6, 24, and 48 h after application of the dressing. The bar chart shows fluorescence measured from the dressed wound, from the wound after removal of the dressing and from the separate, removed dressing. Data are presented as the mean ± SEM ($n = 3$). (B) *In vivo* tissue uptake of TCP-25 from PU discs. Mouse burn wounds were dressed with TCP-25-Cy3 PU. Dressings were removed 6, 24, and 48 h after application and wound tissue was collected. Fluorescence imaging of cryosections was used to detect TCP-25-Cy3 (red). Nuclei (blue) were counterstained with DAPI nuclear stain ($n = 3$). (C) TCP-25 PU dressings were removed from the burn wounds 2, 6, 24, 48 and 72 h after application and eluted in Tris buffer. HPLC was used to detect TCP-25 from the elution. Elution from an unused TCP-25 PU was used as a control. Arrow indicates peak of monomers of TCP-25. (D) Western blot analysis was used to detect TCP-25 in elutions from dressings recovered 2, 6, 24, 48 and 72 h after the application. Purified TCP-25 (1, 2 and 4 µg) was used as a control ($n = 3$). (E) A radial diffusion assay was used to assess bioactivity of TCP-25 in elutions from dressings recovered 2, 6, 24, 48 and 72 h after the application ($n = 3$). (For interpretation of the references to color in this figure legend, the reader is referred to the web version of this article.)

nated with LPS and implanted subcutaneously into mice reporting NF-κB activation. Local inflammatory response was observed when LPS was added to the PU disc, which was abrogated by the PU disc coated with TCP-25 (Fig. 6B). Further, cytokine concentrations were measured in fluid recovered from PU discs and plasma. Discs coated with TCP-25 yielded a significant decrease in the local inflammatory response to the LPS challenge after incubation periods of 8 and 24 h (Fig. 6C). Reductions in plasma levels of TNF-α (after 8 h) and IL-6 and IL-10 (after 24 h) were identified in samples taken from mice implanted with TCP-25-coated discs. Of note, local cytokine levels measured from the fluid recovered from implanted discs were significantly higher than cytokine levels in corresponding plasma. This result clearly demonstrates the importance of assessing local immune responses in addition to systemic/peripheral responses, and also illustrates the feasibility of using PU discs for collection of localized inflammatory exudates. Local and systemic

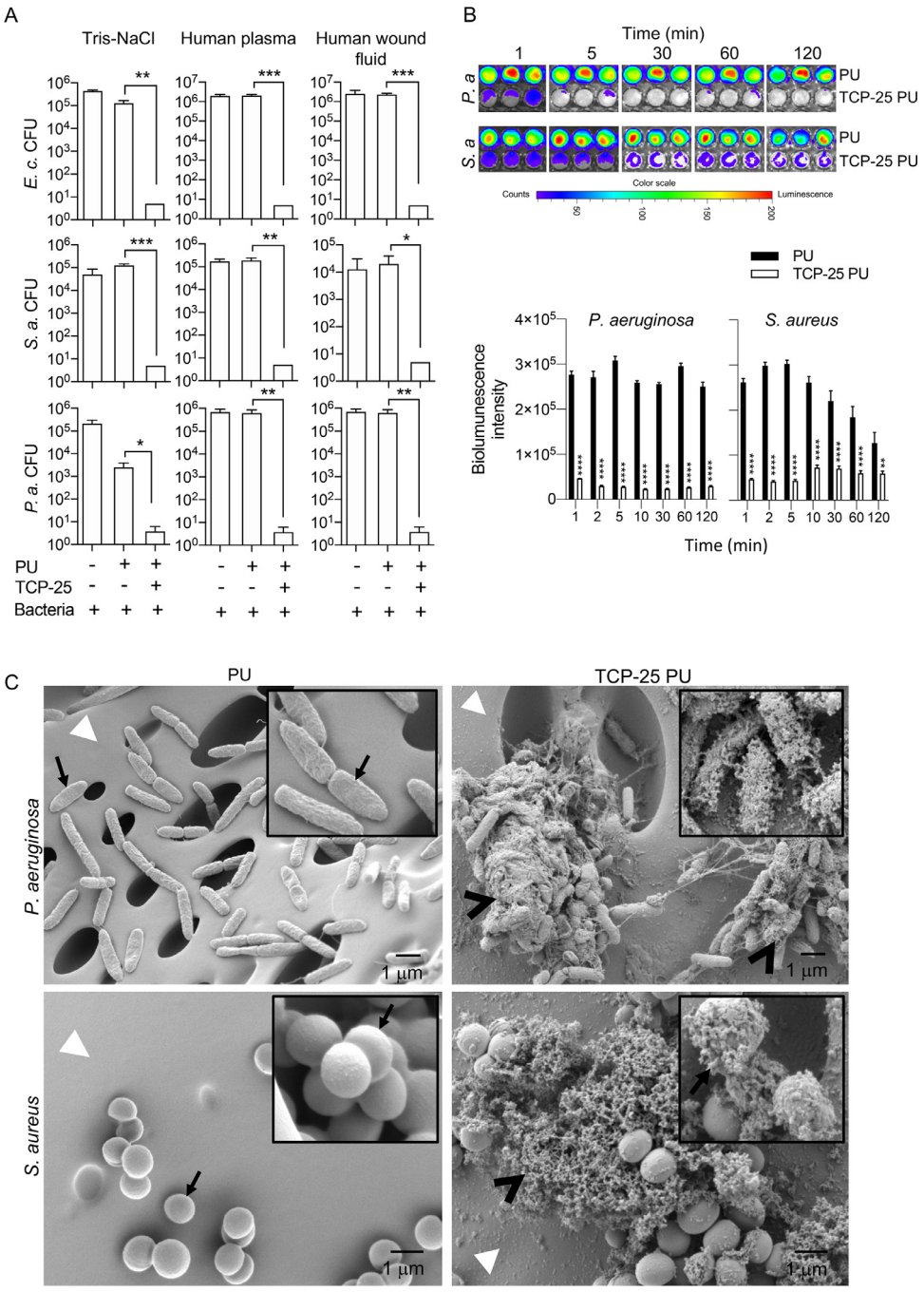

Fig. 4. TCP-25-functionalized PU-discs exert antibacterial properties *in vitro*. (A) Viable count assay for *E. coli* ATCC 25922, *S. aureus* 29213, and *P. aeruginosa* PAO1 after incubating with PU discs with or without TCP-25. Data are represented as the mean ± SD (n=3-4). P values were determined using an unpaired t test. (B) Bioluminescent *P. aeruginosa* or *S. aureus* bacteria were incubated with TCP-25 PU for various time points and the bioluminescent signal was analyzed using bioimaging (IVIS Spectrum). Representative images are shown. Data are represented as the mean ± SEM (n=3). P values were determined using a two-way ANOVA with Sidak's test. (C) Scanning electron microscopy of TCP-25 PU surface with bacteria. Representative SEM images showing the TCP-25 PU surface contaminated with *P. aeruginosa* and *S. aureus*. Arrowhead shows PU surface, arrow shows bacterial cells and open arrowhead shows bacterial lysis and clumping. $^{*}P < 0.05$, $^{**}P < 0.01$, $^{***}P < 0.001$, $^{****}P < 0.0001$. TCP-25 PU are compared with their respective PU controls. *E. c., E. coli; S. a., S. aureus; P. a., P. aeruginosa*.

levels of IL-1β, TGF-β, IL12, and IFN-γ did not show any significant changes.

3.6. TCP-25 blocks endotoxin induced neutrophil and monocyte/macrophage infiltration to the implantation site

The majority of cells isolated from the tissues surrounding the discs were viable even after 24 h (Fig. 7A). However, cells recovered from the PU discs showed poor viability, which might be due to the harsh method for recovering the cells from porous PU discs. The percentage of CD11b-positive cells among the viable cells recovered from the PU discs was 5-10 times lower than in those recovered from the surrounding tissue. The low proportion of CD11b-positive cells in PU disc might be due to the inability of our method to retrieve adhered cells from PU discs. The presence of TCP-25 in the implanted PU discs was associated with reductions in neutrophils and monocytes to levels observed in groups

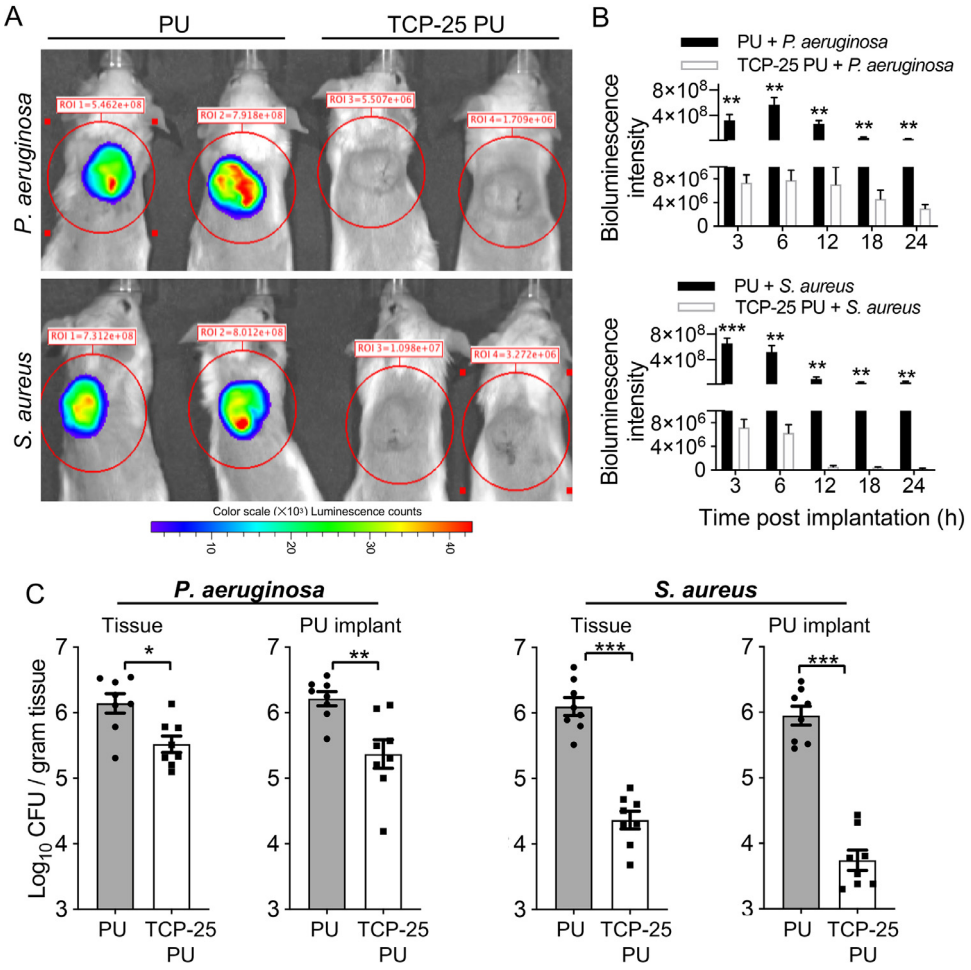

Fig. 5. TCP-25-functionalized PU-discs show antibacterial properties in an experimental mouse model of implant infection (A) Bacterial bioluminescence intensity visualized using IVIS bioimaging. Representative light emission intensity heat-map overlays are shown for the 3 h time point. (B) Bioluminescence intensity emitted by the bacteria was measured by IVIS imaging. Data are represented as the mean ± SD (n=4-5 mice per group). P values were determined using unpaired t tests. TCP-25 PU are compared with their respective PU controls. (C) PU discs alone or coated with TCP-25 were implanted subcutaneously and contaminated with 10^5 CFUs of *P. aeruginosa* Xen41 or *S. aureus* SAP229. Mice were sacrificed 24 h after implantation and CFUs were determined in PU discs and the surrounding tissue, respectively. Data are represented as the mean ± SEM (n=8 mice per group). P values were determined using unpaired t tests. $^{*}P < 0.05$, $^{**}P < 0.01$, $^{***}P < 0.001$.

that were not treated with LPS. The presence of TCP-25 yielded no change in cell infiltration between the groups (Fig. 7A).

A reduction in neutrophil and macrophage invasion in the skin surrounding the implanted TCP-25 PU discs was demonstrated using immunofluorescence microscopy (Fig. 7B). No apparent adverse tissue reactions, such as soft tissue necrosis or vascular changes in response to the TCP-25-coated discs were identified by histology analysis (Fig. 7B). The skin surrounding the LPS-contaminated PU discs showed a minor increase in cellularity, which was not detected in the skin surrounding the TCP-25 PU material. A similar degree of surgery-related adipocyte damage (fat necrosis) was observed in all three groups (sham treated controls, LPS + PU, LPS + PU TCP-25).

3.7. Effects of TCP-25 PU discs in a porcine partial thickness wound model

After demonstrating anti-infective and anti-inflammatory properties of TCP-25 PU *in vitro* and in experimental mouse models, we next wanted to evaluate effects of TCP-25 PU in a model that mimics a clinical situation in which treatment is applied in relation to surgery and bacterial contamination. The major pathogen causing surgical site infections in those clinical situations is *S. aureus* [1]. Of relevance is that TCP-25 targets this bacterium as well as its extracellular TLR-agonists, LTA and PGN [22,23]. With this as background, we decided to use a wound model in Göttingen minipigs which was inoculated with *S. aureus*, thus simulating a surgical situation of wound contamination followed by treatment [23]. Dermatome-induced surgical wounds were inoculated with *S. aureus*, followed by application of the PU dressing coated with TCP-25 (Fig. 8A). PU dressing alone was used for control. Dressings were changed every day until the end of study at day 4 (Fig. 8B). After 4 days, untreated control wounds showed clear signs of infection and inflammation (Fig. 8C). Application of TCP-25 PU treated the bacterial infection resulting in improved clinical score (Fig. 8C), reduced wound bacterial counts and lower levels of TNF-α (Fig. 8D, E). TCP-25 PU dressings recovered from the wounds had a significant reduction in bacterial load (Supplementary Fig. 7). Histological analysis of TCP-25 PU-treated wounds showed reduced inflammatory signs and significantly better histology score at the tissue compared to the infected untreated wounds (Fig. 8F). Notably, reduction of the levels of TNF-α occurred even before the antibacterial effects of TCP-25 PU were observed in treated wounds, highlighting that TCP-25 PU treatment could reduce cytokines independently of bacterial presence. This may be because TCP-25 binds to and neutralizes bacterial LPS [18], interacts directly with monocytes and macrophages and inhibits NF-κB activation in response to several microbe-derived agonists [18,22], and also binds

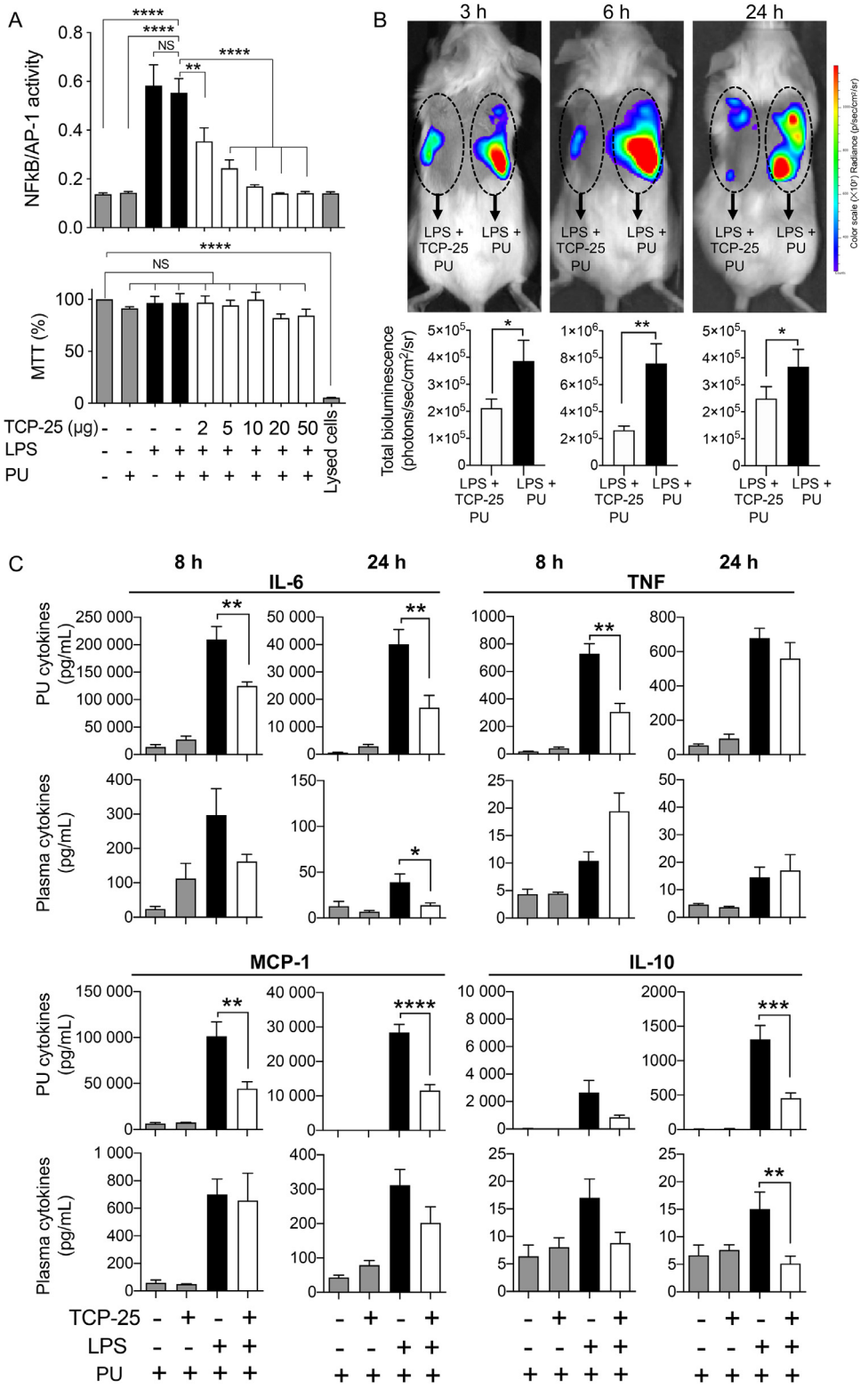

Fig. 6. TCP-25 coated PU discs block endotoxin-induced pro-inflammatory responses *in vitro* and *in vivo*. (A) Activation of NF-κB and AP-1 as determined by measuring the production of secreted alkaline phosphatase using THP1-Xblue™-CD14 reporter cells (upper panel). The percentage of viable cells quantified with MTT assay (lower panel). Lysed cells were used as a positive control for MTT assay. Data are represented as the mean ± SEM (n=3). P values were determined using a one-way ANOVA. (B) *In vivo* inflammation imaging by IVIS in NF-κB reporter mice. TCP-25 PU discs were contaminated with LPS and subcutaneously deposited on the back of transgenic BALB/c Tg(NF-κB-RE-luc)-Xen reporter mice. *In vivo* bioimaging of NF-κB reporter gene expression was performed using the IVIS Spectrum system. Representative images show bioluminescence at 3, 6, and 24 h post subcutaneous deposition. Bar charts show measured light intensity emitted from these reporter mice. Data are presented as the mean ± SEM (n = 6-7 mice per group). P values were determined using unpaired t tests. (C) Cytokine levels in plasma and fluid extracted from implanted PU discs after 8 or 24 h. The discs were subcutaneously implanted and contaminated by addition of LPS. Animals were sacrificed at 8 and 24 h after implantation. Data are presented as the mean ± SD (n = 3-4 mice per group). P values were determined using a one-way ANOVA with Tukey's test. $^{*}P < 0.05$, $^{**}P < 0.01$, $^{***}P < 0.001$, $^{****}P < 0.0001$. NS, non-significant.

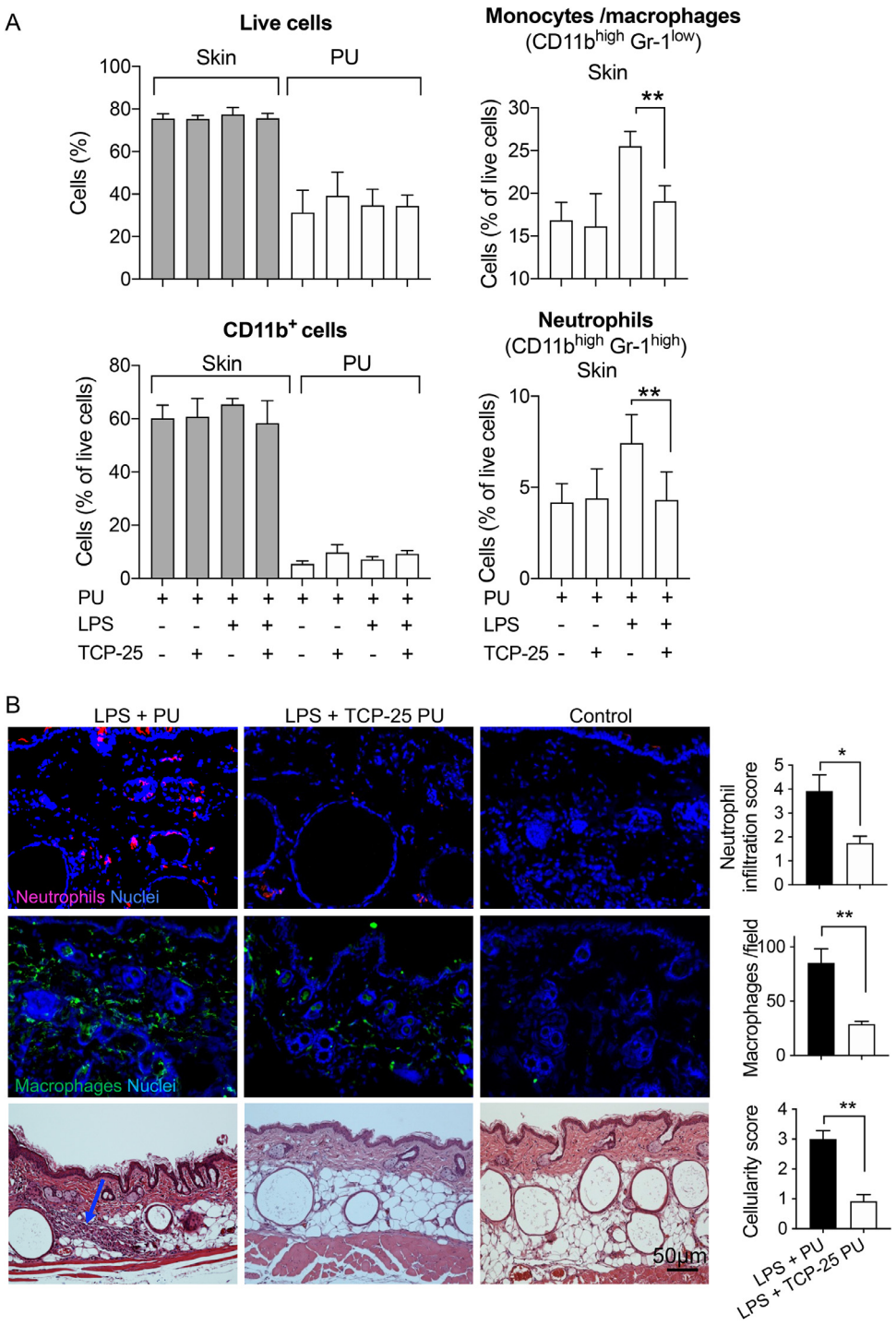

Fig. 7. TCP-25 blocks endotoxin induced neutrophil and monocyte/macrophage infiltration to the implantation site. (A) Flow cytometry analysis of cells recovered from the implanted PU material and surrounding skin tissue 24 h post-implantation of LPS contaminated PU-discs. Cells were stained with 7-AAD stain and CD11b-Alexa fluor-647, and Gr-1-Alexa fluor-488 antibodies. Graphs represent live cells (% of total cells), $CD11b^{+}$ cells (% of live cells), $CD11b^{high}$ $Gr\text{-}1^{low}$ (monocytes/macrophages; % of live cells), and $CD11b^{high}$ $Gr\text{-}1^{high}$ cells (neutrophils; % of live cells). Data are presented as the mean ± SD ($n = 3$). P values were determined using a Mann-Whitney U test. $^{*}P < 0.05$, $^{**}P < 0.01$. (B) Histological analysis of the tissue surrounding the implanted PU 24 h post-implantation of LPS-contaminated PU discs. Immunofluorescence staining of the skin tissue surrounding the PU material. Sections were stained with primary antibodies against neutrophils (upper panel) and macrophages (middle panel). DAPI was used as a nuclear counterstain (blue). Representative images at 40 × magnification of sections stained with hematoxylin and eosin (lower panel). Arrow indicates inflammatory infiltrates. Histogram shows neutrophil infiltration score and macrophage count from immunostaining and cellularity score from H&E stained tissue. Data are presented as the mean ± SD (n = 3-4 mice per group). P values were determined using an unpaired t test. Scale bar, 50 µm. (For interpretation of the references to color in this figure legend, the reader is referred to the web version of this article.)

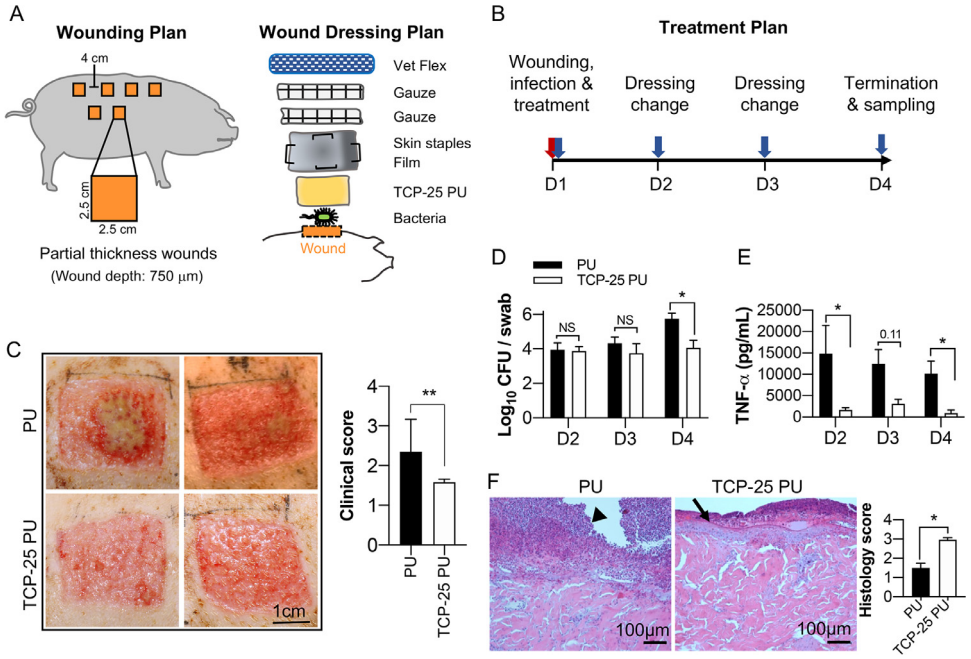

Fig. 8. Effects of TCP-25 PU in a porcine partial thickness wound model. (A) Schematic illustrating the wounding and wound dressing plan in Göttingen minipigs. Using a dermatome, partial thickness wounds were created on the backs of minipigs, followed by inoculation with *S. aureus* (10^7 CFU per wound). After inoculation, wounds were covered with TCP-25 PU followed by a transparent breathable fixation dressing secured with skin staples. Finally, two layers of sterile cotton gauze were secured with adhesive tape and topped with a layer of flexible self-adhesive bandage. (B) Treatment regimen for minipig wounds. (C) Representative photographic images of wounds after the treatment regimen. Wounds infected with *S. aureus* were treated every day with TCP-25 PU. Control wounds were treated with PU without TCP-25 (Scale bar, 1 cm). Bar chart shows clinical scoring of wounds after the treatment regimen. Data are presented as the medians with 95% confidence intervals ($n = 6$ wounds for PU, $n = 6$ wounds for TCP-25 PU from 2 pigs). *P* values were determined using a Mann-Whitney U test. (D) Microbiological analysis of wounds from days 2, 3, and 4. Data are presented as the mean ± SEM ($n = 6$ wounds for PU, $n = 6$ wounds for TCP-25 PU from 2 pigs). *P* values were determined using a Mann-Whitney U test. (E) Analysis of wound fluid cytokine collected on days 2, 3, and 4. Data are presented as the mean ± SEM ($n = 6$ wounds for PU, $n = 4$ wounds for TCP-25 PU from 2 pigs). *P* values were determined using a Mann-Whitney U test. (F) Representative photomicrographs of wound biopsy sections stained with H&E. Arrowhead show hyper-inflammatory condition and severe tissue destruction of the wound. Arrow shows wound re-epithelization. The bar chart shows histological scoring of H&E stained sections. Data are presented as the mean ± SEM ($n = 4$ wounds for PU, $n = 4$ wounds for TCP-25 PU from 2 pigs). *P* values were determined using a Mann-Whitney U test. $^*P < 0.05$, $^{**}P < 0.01$; NS, non-significant.

to the LPS-binding hydrophobic pocket of CD14 [18]. Finally, the hemolytic activity of TCP-25 PU was investigated and the results showed that hemolysis even at highest concentration was less than 10% suggesting that the TCP-25 PU is biocompatible (Supplementary Fig. 8).

4. Discussion

Taken together, this study demonstrates for the first time that it is possible to target both bacteria, as well as the accompanying infection-induced inflammation at the local tissue level with the delivery of host defense peptide TCP-25 from a PU-based material. Importantly, TCP-25 reduced excessive levels of local cytokines, demonstrating its capacity to not only reduce bacterial loads, but also the local inflammatory response. This is of high relevance, since it is well established from a clinical and experimental perspective that bacterial infection complicates and delays wound healing in acute as well as non-healing wounds [34,35]. Of importance is also that studies have shown that presence of low level of bacterial products in the wound bed causes increased leukocyte infiltration and activation [36,37] as well as role of TLR-4 activation in the wound healing process [9,38].

Long-term wound models in small rodents are sub-optimal due to the anatomical and physiological differences between mouse and human skin, but allow for easy and robust testing of antimicrobial and anti-inflammatory properties in acute settings [39,40]. We therefore used an experimental mouse model of subcutaneous infection, rather than an open wound, which enabled us to maintain a controlled environment and quantify the immediate local immune response by recovery of the implanted discs and measuring levels of cytokines as well as cellular influx to the site of implantation. In this context, it is noteworthy that Schutte et al. detected increased cytokine levels in response to implanted steel cages with LPS-impregnated PU material [41], further motivating the use of a subcutaneous model. Sterile sub-cutaneous implantation was particularly useful in order to separately demonstrate antimicrobial and anti-endotoxic properties of the TCP-25 functionalized PU material. Detection of significantly higher cytokine levels locally in the PU discs compared with the observed systemic levels may be due to the obvious localization of the inflammatory process, resulting in a high local release of inflammatory cytokines. In agreement, we noticed infiltration of inflammatory cells in the PU material. Moreover, due to the absorptive properties of the PU, increased accumulation of inflammatory fluid may also have contributed to the observed effects. The finding that TCP-25 PU had a stronger antibacterial effect against *S. aureus* than it did against *P. aeruginosa* confirms our previous observation that MIC values of TCP-25 for *S. aureus* are significantly lower than that for *P. aeruginosa* [23] and can be attributed to the differences in bacterial plasma membrane characteristics between the two species [42].

Wound healing requires a coordinated effort of immune response and regeneration, going through phases of inflammation, proliferation, and remodeling/scar formation. In the event of infection, inflammation, an important part of the wound-healing response, is exacerbated and prolonged leading to excessive cytokine production and neutrophil and macrophage infiltration. Collateral tissue damage associated with the neutrophil activity and release of an array of proteases and other enzymes affect later events in the repair process with long-lasting effects on the speed of repair, re-epithelization and scarring. Additionally, these proteases

can also degrade the extracellular matrix to a point where tissue destruction causes persistent inflammation and perpetuating tissue damage [43–46]. In the same context there is ample evidence of connection between presence of LPS [47] as well as a sustained presence of pro-inflammatory monocytes, with compromised wound repair [46]. In this perspective, it is therefore notable that TCP-25-coated PU significantly reduced the numbers of neutrophils and macrophages being recruited to the site after stimulation with endotoxins. In contrast to the previous findings, where cyclooxygenase inhibitors were used to ameliorate the endotoxin-induced excessive inflammation, TCP-25 did not reduce the amount of cellular infiltrates below the levels occurring in a sterile and endotoxin free environment [37,46]. This finding, together with the *in vitro* toxicity data altogether implies that presence of TCP-25 in the implanted disc is well tolerated and does not skew local reaction to the material. Tolerance of TCP-25 PU is important since the majority of antimicrobial agents that are not antibiotics, can be cytotoxic or poorly tolerated by bystander cells [48,49].

While the need to ameliorate excessive inflammation in infected wounds is not debated, there are conflicting reports surrounding the use of anti-inflammatory agents like non steroid and steroid kinase inhibitors and their impact on the healing process [36,50–54]. Though steroid and non-steroid inhibitors (NSAID) are highly effective, their application as acute wound anti-inflammatory therapy has major drawbacks including inhibition of a physiological antimicrobial response and reduction of re-epithelization and tissue regeneration. The fact that TCP-25 selectively binds to bacterial products such as LPS, LTA, and PGN and blocks the resulting TLR interaction, and does not have the inhibitory effects on other downstream signaling pathways [18,22] as observed for steroids or NSAID [55–57], should therefore reduce the risk for unwanted side-effects.

In the present work we used a high dose of LPS, far higher than low dose described by other reports [58] in order to demonstrate a proof of principle that TCP-25 functionalized PU material can scavenge high amounts of LPS rapidly. The LPS levels in an infected wound bed are likely lower, however, the continuous release of bacterial compounds after a single TCP-25 application to an infected area needs to be considered and accounted for. As we show here and in previous studies, TCP-25 efficiently kills a broad range of bacteria by cell wall lysis [20,32], and the simultaneous neutralizing action on bacterial wall products such as LPS, LTA, and PGN of the peptide prevents excessive inflammatory responses both *in vitro* and *in vivo* [19,59]. This is crucial, as bacterial toxins released during this process would additionally increase and prolong the inflammatory reaction at the infection site.

Porcine wound models are considered as the most relevant preclinical models for human translation [60]. In a minipig short-term partial thickness contaminated wound model, we observed that the TCP-25 PU was efficient in abrogating infection with *S. aureus*. Importantly, TCP-25 PU treated wound showed a decrease in the levels of TNF-α. Notably, these data are in agreement with previous observations that TCP-25 does not only block endotoxin responses, but also TLR 2 and 4 activations in response to stimulus with PGN and LTA, respectively [19,22]. This finding, however, arguably could depend on the concomitant reductions in bacterial numbers in the wound which may lead to reduced toxin release into the wound area causing less inflammation. However, the observation that TNF-α concentrations were reduced even before bacterial numbers were affected lends support for a separate anti-inflammatory action of TCP-25 PU *in vivo*, acting in parallel with its antibacterial effects.

From a peptide delivery perspective, it was important that PU should not interfere with the flexible conformation of TCP-25 which is essential for its interaction with bacteria and host cells [18,32,61]. To study the impact of PU on TCP-25, we employed a combination of bioassays and structural analysis using CD and intrinsic fluorescence analysis. The results showed that TCP-25 released from PU retained both its flexible conformation in buffer and helix inducing-capacity in presence of LPS, compatible with its antibacterial and anti-inflammatory actions. Moreover, TCP-25 PU discs continuously released TCP-25 to the wound site for at least 48 h. We also show that TCP-25 is retained in PU discs for at least 72 h and remains bioactive during this time.

Various antimicrobials such as antibiotics or antiseptics are currently in clinical use for the treatment and prevention of wound and implant-related infections [5]. However, anti-infective treatments also targeting specific microbial products are not currently available. Nevertheless, there is a great interest in developing new anti-inflammatory compounds to aid in wound healing [62,63]. The present study demonstrates a proof of concept that TCP-25, exhibiting dual antimicrobial and anti-inflammatory functions, could be a compound of interest in the development of functionalized materials for wound and surgical infections. Future studies in relevant preclinical models of bacterial wound infection are mandated in order to investigate the dose-response relationship related to various TCP-25 coating concentrations.

5. Conclusion

We here demonstrate a dual action wound dressing concept where a PU material coated with the peptide TCP-25 is able to counteract bacterial infection and the accompanying inflammation *in vitro* and in experimental infection models in mice and minipigs.

Funding sources

This work was supported by grants from Alfred Österlunds Foundation, Edvard Welanders Stiftelse and Finsenstiftelsen, The Crafoord foundation, Knut and Alice Wallenberg Foundation, Thelma Zoégas Foundation, the Royal Physiographic Society, the Swedish Strategic Research Foundation, Vinnova, the Swedish Government Funds for Clinical Research (ALF), and the Swedish Research Council (2012-1883, 2017-02341).

Declaration of Competing Interest

Dr. Schmidtchen is a founder of in2cure AB, a company developing anti-inflammatory peptides for therapeutic applications. M. Puthia has received consultation fees from in2cure AB.

Acknowledgements

We thank Drs. Kristina Hamberg and Sofia Almqvist, Mölnlycke Health Care AB (Göteborg, Sweden) for providing the Mepilex PU material, and for fruitful discussions and advice in relation to the porcine wound models. We thank Elzbieta Eriksson (BMC, Lund University) for assistance in the animal studies and Susanne Strömblad (Bioimaging Center, Lund University) for histology support. Lund University Bioimaging Centre (LBIC), Lund University, is gratefully acknowledged for providing experimental resources. We thank Jane Fisher for editing of the manuscript.

Supplementary materials

Supplementary material associated with this article can be found, in the online version, at doi:10.1016/j.actbio.2021.04.045.

References

[1] K. Saleh, A. Schmidtchen, Surgical site infections in dermatologic surgery: etiology, pathogenesis, and current preventative measures, Dermatol. Surg. 41 (5) (2015) 537–549.
[2] J.C. Dumville, C.J. Walter, C.A. Sharp, T. Page, Dressings for the prevention of surgical site infection, Cochrane Database. Syst. Rev. (7) (2011) CD003091.
[3] C.K. Sen, G.M. Gordillo, S. Roy, R. Kirsner, L. Lambert, T.K. Hunt, F. Gottrup, G.C. Gurtner, M.T. Longaker, Human skin wounds: a major and snowballing threat to public health and the economy, Wound Repair Regen. 17 (6) (2009) 763–771.
[4] S.B. Goodman, Z. Yao, M. Keeney, F. Yang, The future of biologic coatings for orthopaedic implants, Biomaterials 34 (13) (2013) 3174–3183.
[5] H.J. Busscher, H.C. van der Mei, G. Subbiahdoss, P.C. Jutte, J.J. van den Dungen, S.A. Zaat, M.J. Schultz, D.W. Grainger, Biomaterial-associated infection: locating the finish line in the race for the surface, Sci. Transl. Med. 4 (153) (2012) 153rv10.
[6] J. Gallo, M. Holinka, C.S. Moucha, Antibacterial surface treatment for orthopaedic implants, Int. J. Mol. Sci. 15 (8) (2014) 13849–13880.
[7] E. Kolaczkowska, P. Kubes, Neutrophil recruitment and function in health and inflammation, Nat. Rev. Immunol. 13 (3) (2013) 159–175.
[8] F. Grinnell, M. Zhu, Fibronectin degradation in chronic wounds depends on the relative levels of elastase, alpha1-proteinase inhibitor, and alpha2-macroglobulin, J. Investig. Dermatol. 106 (2) (1996) 335–341.
[9] M.R. Dasu, R.R. Isseroff, Toll-like receptors in wound healing: location, accessibility, and timing, J. Investig. Dermatol. 132 (8) (2012) 1955–1958.
[10] P. D'Arpa, K.P. Leung, Toll-Like Receptor Signaling in Burn Wound Healing and Scarring, Adv. Wound Care 6 (10) (2017) 330–343 (New Rochelle).
[11] M. Rani, S.E. Nicholson, Q. Zhang, M.G. Schwacha, Damage-associated molecular patterns (DAMPs) released after burn are associated with inflammation and monocyte activation, Burns 43 (2) (2017) 297–303.
[12] S.A. Eming, T. Krieg, J.M. Davidson, Inflammation in wound repair: molecular and cellular mechanisms, J. Investig. Dermatol. 127 (3) (2007) 514–525.
[13] S.A. Eming, P. Martin, M. Tomic-Canic, Wound repair and regeneration: mechanisms, signaling, and translation, Sci. Transl. Med. 6 (265) (2014) 265sr6.
[14] R. Medzhitov, T. Horng, Transcriptional control of the inflammatory response, Nat. Rev. Immunol. 9 (10) (2009) 692–703.
[15] M. Puthia, I. Ambite, C. Cafaro, D. Butler, Y. Huang, N. Lutay, G. Rydstrom, B. Gullstrand, B. Swaminathan, A. Nadeem, B. Nilsson, C. Svanborg, IRF7 inhibition prevents destructive innate immunity-A target for nonantibiotic therapy of bacterial infections, Sci. Transl. Med. 8 (336) (2016) 336ra59.
[16] J. Petrlova, F.C. Hansen, M.J.A. van der Plas, R.G. Huber, M. Morgelin, M. Malmsten, P.J. Bond, A. Schmidtchen, Aggregation of thrombin-derived C-terminal fragments as a previously undisclosed host defense mechanism, Proc. Natl. Acad. Sci. USA 114 (21) (2017) E4213–E4222.
[17] M.J. van der Plas, R.K. Bhongir, S. Kjellstrom, H. Siller, G. Kasetty, M. Morgelin, A. Schmidtchen, Pseudomonas aeruginosa elastase cleaves a C-terminal peptide from human thrombin that inhibits host inflammatory responses, Nat. Commun. 7 (2016) 11567.
[18] R. Saravanan, D.A. Holdbrook, J. Petrlova, S. Singh, N.A. Berglund, Y.K. Choong, S. Kjellstrom, P.J. Bond, M. Malmsten, A. Schmidtchen, Structural basis for endotoxin neutralisation and anti-inflammatory activity of thrombin-derived C-terminal peptides, Nat. Commun. 9 (1) (2018) 2762.
[19] M. Kalle, P. Papareddy, G. Kasetty, M. Morgelin, M.J. van der Plas, V. Rydengard, M. Malmsten, B. Albiger, A. Schmidtchen, Host defense peptides of thrombin modulate inflammation and coagulation in endotoxin-mediated shock and Pseudomonas aeruginosa sepsis, PLoS One 7 (12) (2012) e51313.
[20] P. Papareddy, V. Rydengard, M. Pasupuleti, B. Walse, M. Morgelin, A. Chalupka, M. Malmsten, A. Schmidtchen, Proteolysis of human thrombin generates novel host defense peptides, PLoS Pathog. 6 (4) (2010) e1000857.
[21] R. Saravanan, S.S. Adav, Y.K. Choong, M.J.A. van der Plas, J. Petrlova, S. Kjellstrom, S.K. Sze, A. Schmidtchen, Proteolytic signatures define unique thrombin-derived peptides present in human wound fluid *in vivo*, Sci. Rep. 7 (1) (2017) 13136.
[22] F.C. Hansen, M. Kalle-Brune, M.J. van der Plas, A.C. Stromdahl, M. Malmsten, M. Morgelin, A. Schmidtchen, The thrombin-derived host defense peptide GKY25 inhibits endotoxin-induced responses through interactions with lipopolysaccharide and macrophages/monocytes, J. Immunol. 194 (11) (2015) 5397–5406.
[23] M. Puthia, M. Butrym, J. Petrlova, A.C. Strömdahl, M. Andersson, S. Kjellström, A. Schmidtchen, A dual-action peptide-containing hydrogel targets wound infection and inflammation, Sci. Transl. Med. 12 (524) (2020).
[24] C. Del Amo, A. Perez-Valle, E. Perez-Zabala, K. Perez-Del-Pecho, A. Larrazabal, A. Basterretxea, P. Bully, I. Andia, Wound dressing selection is critical to enhance platelet-rich fibrin activities in wound care, Int. J. Mol. Sci. 21 (2) (2020).
[25] T. Maver, L. Gradisnik, D.M. Smrke, K. Stana Kleinschek, U. Maver, Systematic evaluation of a diclofenac-loaded carboxymethyl cellulose-based wound dressing and its release performance with changing ph and temperature, AAPS Pharm. Sci. Tech. 20 (1) (2019) 29.
[26] J.D. Morrisett, J.S. David, H.J. Pownall, A.M. Gotto, Interaction of an apolipoprotein (apoLP-alanine) with phosphatidylcholine, Biochemistry 12 (7) (1973) 1290–1299.
[27] J.L. Medina, A.B. Fourcaudot, E.A. Sebastian, R. Shankar, A.W. Brown, K.P. Leung, Standardization of deep partial-thickness scald burns in C57BL/6 mice, Int. J. Burns Trauma 8 (2) (2018) 26–33.
[28] G. Petruk, J. Petrlova, F. Samsudin, R.D. Giudice, P.J. Bond, A. Schmidtchen, Concentration- and pH-dependent oligomerization of the thrombin-derived C-terminal peptide TCP-25, Biomolecules 10 (11) (2020).
[29] G. Kasetty, M. Kalle, M. Morgelin, J.C. Brune, A. Schmidtchen, Anti-endotoxic and antibacterial effects of a dermal substitute coated with host defense peptides, Biomaterials 53 (2015) 415–425.
[30] S. Dhivya, V.V. Padma, E. Santhini, Wound dressings - a review, Biomedicine 5 (4) (2015) 22 (Taipei).
[31] Z. Lateef, G. Stuart, N. Jones, A. Mercer, S. Fleming, L. Wise, The cutaneous inflammatory response to thermal burn injury in a murine model, Int. J. Mol. Sci. 20 (3) (2019).
[32] G. Kasetty, P. Papareddy, M. Kalle, V. Rydengard, M. Morgelin, B. Albiger, M. Malmsten, A. Schmidtchen, Structure-activity studies and therapeutic potential of host defense peptides of human thrombin, Antimicrob. Agent. Chemother. 55 (6) (2011) 2880–2890.
[33] S. Gupta, G.V. Prasad, A. Mukhopadhaya, Vibrio cholerae porin OmpU induces caspase-independent programmed cell death upon translocation to the host cell mitochondria, J. Biol. Chem. 290 (52) (2015) 31051–31068.
[34] D.G. Metcalf, P.G. Bowler, Biofilm delays wound healing: a review of the evidence, Burns Trauma 1 (1) (2013) 5–12.
[35] K. Rahim, S. Saleha, X. Zhu, L. Huo, A. Basit, O.L. Franco, Bacterial contribution in chronicity of wounds, Microb. Ecol. 73 (3) (2017) 710–721.
[36] Z. Metzger, D. Nitzan, S. Pitaru, T. Brosh, S. Teicher, The effect of bacterial endotoxin on the early tensile strength of healing surgical wounds, J. Endod. 28 (1) (2002) 30–33.
[37] M. Singh, K. Nuutila, I. Sinha, E. Eriksson, Endotoxin-induced inflammation in a rodent model up-regulates IL-1a expression and CD45+ leukocyte recruitment and increases the rate of reepithelialization and wound closure, Wound Repair Regen. 24 (5) (2016) 820–828.
[38] L. Chen, L.A. DiPietro, Toll-like receptor function in acute wounds, Adv. Wound Care 6 (10) (2017) 344–355 (New Rochelle).
[39] S.M. Behar, C.J. Martin, C. Nunes-Alves, M. Divangahi, H.G. Remold, Lipids, apoptosis, and cross-presentation: links in the chain of host defense against Mycobacterium tuberculosis, Microbe. Infect. 13 (8-9) (2011) 749–756.
[40] V.W. Wong, M. Sorkin, J.P. Glotzbach, M.T. Longaker, G.C. Gurtner, Surgical approaches to create murine models of human wound healing, J. Biomed. Biotechnol. 2011 (2011) 969618.
[41] R.J. Schutte, L. Xie, B. Klitzman, W.M. Reichert, *In vivo* cytokine-associated responses to biomaterials, Biomaterials 30 (2) (2009) 160–168.
[42] J. Li, J.J. Koh, S. Liu, R. Lakshminarayanan, C.S. Verma, R.W. Beuerman, Membrane active antimicrobial peptides: translating mechanistic insights to design, Front. Neurosci. 11 (2017) 73.
[43] T.A. Wilgus, S. Roy, J.C. McDaniel, Neutrophils and Wound Repair: Positive Actions and Negative Reactions, Adv. Wound Care 2 (7) (2013) 379–388 (New Rochelle).
[44] L.W. Qian, A.B. Fourcaudot, K. Yamane, T. You, R.K. Chan, K.P. Leung, Exacerbated and prolonged inflammation impairs wound healing and increases scarring, Wound Repair Regen. 24 (1) (2016) 26–34.
[45] T.J. Koh, L.A. DiPietro, Inflammation and wound healing: the role of the macrophage, Expert Rev. Mol. Med. 13 (2011) e23.
[46] R. Yuan, S. Geng, K. Chen, N. Diao, H.W. Chu, L. Li, Low-grade inflammatory polarization of monocytes impairs wound healing, J. Pathol. 238 (4) (2016) 571–583.
[47] H. Kawaguchi, A. Hizuta, N. Tanaka, K. Orita, Role of endotoxin in wound healing impairment, Res. Commun. Mol. Pathol. Pharmacol. 89 (3) (1995) 317–327.
[48] M. Bacalum, M. Radu, Cationic antimicrobial peptides cytotoxicity on mammalian cells: an analysis using therapeutic index integrative concept, Int. J. Pept. Res. Ther. 21 (1) (2015) 47–55.
[49] S. Pacor, A. Giangaspero, M. Bacac, G. Sava, A. Tossi, Analysis of the cytotoxicity of synthetic antimicrobial peptides on mouse leucocytes: implications for systemic use, J. Antimicrob. Chemother. 50 (3) (2002) 339–348.
[50] S.G. Vallejo-Heligon, N.L. Brown, W.M. Reichert, B. Klitzman, Porous, dexamethasone-loaded polyurethane coatings extend performance window of implantable glucose sensors *in vivo*, Acta Biomater. 30 (2016) 106–115.
[51] A.S. Wang, E.J. Armstrong, A.W. Armstrong, Corticosteroids and wound healing: clinical considerations in the perioperative period, Am. J. Surg. 206 (3) (2013) 410–417.
[52] K. Anderson, R.L. Hamm, Factors that impair wound healing, J. Am. Coll. Clin. Wound Spec. 4 (4) (2012) 84–91.
[53] H. Khalil, M. Cullen, H. Chambers, M. McGrail, Medications affecting healing: an evidence-based analysis, Int. Wound J. 14 (6) (2017) 1340–1345.
[54] S. Iwamoto, T. Koga, M. Ohba, T. Okuno, M. Koike, A. Murakami, A. Matsuda, T. Yokomizo, Non-steroidal anti-inflammatory drug delays corneal wound healing by reducing production of 12-hydroxyheptadecatrienoic acid, a ligand for leukotriene B4 receptor 2, Sci. Rep. 7 (1) (2017) 13267.
[55] R. Pai, I.L. Szabo, A.Q. Giap, H. Kawanaka, A.S. Tarnawski, Nonsteroidal anti-inflammatory drugs inhibit re-epithelialization of wounded gastric monolayers by interfering with actin, Src, FAK, and tensin signaling, Life Sci. 69 (25-26) (2001) 3055–3071.
[56] R. Broering, M. Montag, M. Jiang, M. Lu, J.P. Sowa, K. Kleinehr, G. Gerken, J.F. Schlaak, Corticosteroids shift the Toll-like receptor response pattern of primary-isolated murine liver cells from an inflammatory to an anti-inflammatory state, Int. Immunol. 23 (9) (2011) 537–544.
[57] T.H. Mogensen, R.S. Berg, S.R. Paludan, L. Ostergaard, Mechanisms of dexamethasone-mediated inhibition of Toll-like receptor signaling induced by Neis-

seria meningitidis and Streptococcus pneumoniae, Infect. Immun. 76 (1) (2008) 189–197.
[58] Y. Zhang, Y. Lu, L. Ma, X. Cao, J. Xiao, J. Chen, S. Jiao, Y. Gao, C. Liu, Z. Duan, D. Li, Y. He, B. Wei, H. Wang, Activation of vascular endothelial growth factor receptor-3 in macrophages restrains TLR4-NF-kappaB signaling and protects against endotoxin shock, Immunity 40 (4) (2014) 501–514.
[59] F.C. Hansen, A.C. Stromdahl, M. Morgelin, A. Schmidtchen, M.J.A. van der Plas, Thrombin-derived host-defense peptides modulate monocyte/macrophage inflammatory responses to gram-negative bacteria, Front Immunol. 8 (2017) 843.
[60] T.P. Sullivan, W.H. Eaglstein, S.C. Davis, P. Mertz, The pig as a model for human wound healing, Wound Repair Regen. 9 (2) (2001) 66–76.
[61] D.A. Holdbrook, S. Singh, Y.K. Choong, J. Petrlova, M. Malmsten, P.J. Bond, N.K. Verma, A. Schmidtchen, R. Saravanan, Influence of pH on the activity of thrombin-derived antimicrobial peptides, Biochim. Biophys. Acta Biomembr. 1860 (11) (2018) 2374–2384.
[62] K.N. Ekdahl, J.D. Lambris, H. Elwing, D. Ricklin, P.H. Nilsson, Y. Teramura, I.A. Nicholls, B. Nilsson, Innate immunity activation on biomaterial surfaces: a mechanistic model and coping strategies, Adv. Drug Deliv. Rev. 63 (12) (2011) 1042–1050.
[63] S. Franz, S. Rammelt, D. Scharnweber, J.C. Simon, Immune responses to implants - a review of the implications for the design of immunomodulatory biomaterials, Biomaterials 32 (28) (2011) 6692–6709.